Available online at www.sciencedirect.com
SCIENCE DIRECT®
International Journal of Solids and Structures 42 (2005) 5460–5490
INTERNATIONAL JOURNAL OF SOLIDS and STRUCTURES
www.elsevier.com/locate/ijsolstr

Higher-order impact modeling of sandwich structures with flexible core

Mijia Yang, Pizhong Qiao *

Advanced Materials and Structures Research Group, Department of Civil Engineering, The University of Akron, Akron, OH 44325-3905, USA

Received 21 September 2004; received in revised form 18 February 2005
Available online 7 April 2005

Abstract

In this study, a higher-order impact model is presented to simulate the response of a soft-core sandwich beam subjected to a foreign object impact. A free vibration problem of sandwich beams is first solved, and the results are validated by comparing with numerical finite element modeling results of ABAQUS and the solution by Frostig and Baruch [Frostig, Y., Baruch, M., 1994. Free vibration of sandwich beams with a transversely flexible core: a high order approach. Journal of Sound and Vibration 176(2), 195–208]. Then a foreign object impact process is incorporated in the higher-order model, and the contact force and deflection history as well as the propagation of transverse normal, shear, and axial stresses during the impact are analyzed and discussed. The validity of the model in the impact response predictions is demonstrated by comparing with finite element solutions of LS-DYNA. The calculated stresses caused by a foreign object impact are then used to assess failure locations, failure time, and failure modes in sandwich beams, which are shown to compare well with the available experimental results. The effects of impact mass, initial velocity, core stiffness, and core height on the impact stresses generated in the beams are discussed. The influences of impact mass and initial velocity on the contact force history are close to those by the linearized impact solution, but the proposed higher-order impact model captures the non-linear impact process and different generated stresses. Compared to the fully backed sandwich case, the core height shows a great influence over the impact process of a simply supported sandwich system, in which the global behavior of the sandwich is dominant; while the core stiffness shows minor effect over the impact process. The higher-order impact model of sandwich beams developed in the study provides accurate predictions of the generated stresses and impact process and can be used effectively in design analysis of anti-impact structures made of sandwich materials.

Keywords: Higher-order sandwich impact theory; Impact; Free vibration; Failure; Stress wave propagation; Symmetric sandwich beams

* Corresponding author. Tel.: +1 330 972 5226; fax: +1 330 972 6020.
E-mail address: qiao@uakron.edu (P. Qiao).

0020-7683/$ - see front matter © 2005 Elsevier Ltd. All rights reserved.
doi:10.1016/j.ijsolstr.2005.02.037

1. Introduction

Sandwich panels are commonly made of soft core in the form of foams or non-metallic light honeycombs that are flexible in the through-the-thickness direction, and they are prevalently used in structural applications due to weight reduction and promising high-energy absorption. The concentrations of transverse normal and shear stresses between the skins and core, caused by impact of foreign objects, such as a drop weight, are very important in the case of sandwich panels with a "soft" compressible core. These stress concentrations in sandwich structures could lead to premature failure at load levels much lower than the predicted failure load determined using classical theories. The flexibility of the low-strength core affects the overall behavior of sandwich structures and prompts stress concentrations in the vicinity of localized loads and at the skin–core interfaces. It yields unequal deflection patterns in the upper and the lower skins as compared to the panels having traditional metallic anti-plane incompressible core, in which the in-plane stresses can be ignored, the transverse shear stress are independent of the vertical coordinate z, and the rigidity in the vertical direction can be considered as infinite (Allen, 1969). A number of theories have been discussed to solve this problem. The traditional elastic foundation models (Thomsen, 1995) were the earliest ones, which could take account of the core deformation and capture the local bending effect. However they neglect the interaction between the shear and the normal stresses within the core required by the equilibrium conditions. Among all the theories, the higher-order sandwich theory developed by Frostig and his coworkers (Frostig et al., 1992; Frostig and Baruch, 1994, 1996; Frostig and Shenar, 1995; Frostig and Thomsen, 2004) and Sokolinsky and Nutt (2002, 2004) were the most promising ones, in which they assumed that the in-plane displacement of the core is non-linear, i.e., the plane section of the core no longer needs to remain as a plane after deformation, and the height of the sandwich could be compressed and extended.

Even though a lot of work has been done to capture the local effects of loading and supporting boundary of a static problem, the dynamic problems associated with these local effects have not been discussed. In particular, the impact damage of sandwich structures due to a drop weight has not been fully analyzed, which is actually very important in utilizing these sandwich systems properly. The impact over sandwich systems was first analyzed by Lee et al. (1993). In their study, an anti-plane sandwich theory was used, and the transient contact force and central deflection histories were analyzed. Tsai et al. (1998) also conducted a study about the impact analysis of a linear sandwich system, and a linear distribution of the in-plane as well as the vertical displacements was assumed; but their model is still a classical model, which could not guarantee the continuity of stresses over the skin–core interfaces, which also raises the question of the equilibrium of stresses in the core. Qiao et al. (2004) recently presented an I-Lam (**I**mpact **Lam**inate) sandwich system as a collision protective structure for highway bridge girders subjected to underneath over-height trucks impact and developed a closed-form solution for a sandwich beam on a Winkler foundation over impact considering the shear-off effect of truck over-height material. Yang and Qiao (2005) also developed a theoretical model for a fully-backed sandwich plate using a two-parameter elastic foundation, and the damage generated by foreign object impact was discussed in detail considering the effects of mass, initial velocity and projectile tip shape. Most recently, Qiao and Yang (2004) further proposed a semi-analytical model for an anti-plane sandwich plate sitting on a solid half space, and the transferred force distributions as well as impact response were studied.

In this study, the impact analysis of sandwich beams based on a higher-order sandwich theory is conducted. A higher-order sandwich theory incorporating the impact process is used to study the local deflection and stress concentration effects of the impact. By excluding the assumptions of linearly distributed displacements (or core's plane sections remaining plane after deformation), both the continuity of stresses over the skin–core interface and the normal compression of the core are taken into consideration, and the stress concentration and stress wave propagation caused by the impact process are analyzed. The transient impact response of the sandwich system is studied, and the dynamic effect of core and various transient

stresses under impact, which are needed to assess the failure time, locations and modes in a sandwich system, are discussed in detail.

2. Theoretical formulation

2.1. Dynamics of a sandwich beam system

First, consider a sandwich beam based on the plane stress conditions (in the xz plane) and the coordinate system given in Fig. 1, the equation of motion of a sandwich beam is given as

$$\begin{aligned}
\frac{\partial \sigma_{xx}^{t}}{\partial x}+\frac{\partial \sigma_{xz}^{t}}{\partial z}&=\rho_{t}\frac{\partial^{2}u_{t}}{\partial t^{2}}\\
\frac{\partial \sigma_{xz}^{t}}{\partial x}+\frac{\partial \sigma_{zz}^{t}}{\partial z}&=\rho_{t}\frac{\partial^{2}w_{t}}{\partial t^{2}}\\
\frac{\partial \sigma_{xx}^{c}}{\partial x}+\frac{\partial \sigma_{xz}^{c}}{\partial z}&=\rho_{c}\frac{\partial^{2}u_{c}}{\partial t^{2}}\\
\frac{\partial \sigma_{xz}^{c}}{\partial x}+\frac{\partial \sigma_{zz}^{c}}{\partial z}&=\rho_{c}\frac{\partial^{2}w_{c}}{\partial t^{2}}\\
\frac{\partial \sigma_{xx}^{b}}{\partial x}+\frac{\partial \sigma_{xz}^{b}}{\partial z}&=\rho_{b}\frac{\partial^{2}u_{b}}{\partial t^{2}}\\
\frac{\partial \sigma_{xz}^{b}}{\partial x}+\frac{\partial \sigma_{zz}^{b}}{\partial z}&=\rho_{b}\frac{\partial^{2}w_{b}}{\partial t^{2}}
\end{aligned} \tag{1}$$

where, w_t, w_c, and w_b are the vertical displacements of the top face sheet, core material, and bottom face sheet, respectively; u_t, u_c, u_b are the horizontal displacements of the top face sheet, core, and bottom face sheet; σ_{xx}, σ_{xz}, σ_{zz} are the components of a stress tensor at a point (τ is later used in this paper instead of σ_{xz}^{c} for simplicity), and the subscripts t, c, and b represent the top face sheet, core, and bottom face sheet, respectively; and ρ_t, ρ_c, and ρ_b are the material density of the top face sheet, core material and bottom face sheet.

2.1.1. Model A: Without the dynamic effect of core

In many sandwich systems, the core is designed to be light compared to that of the face sheets, which makes the mass inertia of the core material much less than that of the face sheets and sometimes can be

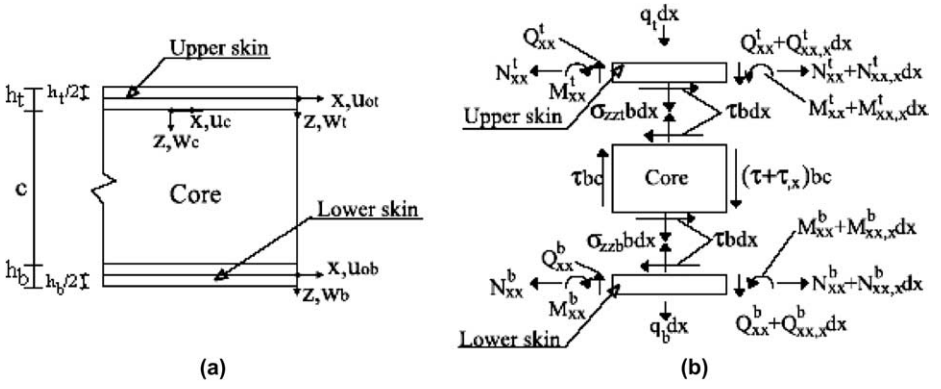

Fig. 1. The coordinate system of sandwich beam: (a) geometry and coordinates, (b) internal resultants and stresses.

omitted. Most of core materials in sandwich construction are made of either low density foams or honeycomb structures, and for simplified analysis, the dynamic effect (i.e., the horizontal and vertical vibration) of the core is often not included. Model A is designed for this type of sandwich beams that the dynamic effect of the core is neglected. Integration of the equations for the face sheets in Eq. (1) yields

$$\begin{aligned}
&\frac{\partial N_{xx}^{\mathrm{t}}}{\partial x}+\sigma_{xz}^{\mathrm{t}}(x,z=h_{\mathrm{t}}/2)-\sigma_{xz}^{\mathrm{t}}(x,z=-h_{\mathrm{t}}/2)=0\\
&\frac{\partial^2 M_{xx}^{\mathrm{t}}}{\partial x^2}+\sigma_{zz}^{\mathrm{t}}(x,z=h_{\mathrm{t}}/2)-\sigma_{zz}^{\mathrm{t}}(x,z=-h_{\mathrm{t}}/2)+\frac{\partial\sigma_{xz}}{\partial x}\frac{h_{\mathrm{t}}}{2}=\int_{-h_{\mathrm{t}}/2}^{h_{\mathrm{t}}/2}\rho_{\mathrm{t}}\,\mathrm{d}z\frac{\partial^2 w_{\mathrm{t}}}{\partial t^2}\\
&\frac{\partial N_{xx}^{\mathrm{b}}}{\partial x}+\sigma_{xz}^{\mathrm{b}}(x,z=h_{\mathrm{b}}/2)-\sigma_{xz}^{\mathrm{b}}(x,z=-h_{\mathrm{b}}/2)=0\\
&\frac{\partial^2 M_{xx}^{\mathrm{b}}}{\partial x^2}+\sigma_{zz}^{\mathrm{b}}(x,z=h_{\mathrm{b}}/2)-\sigma_{zz}^{\mathrm{b}}(x,z=-h_{\mathrm{b}}/2)+\frac{\partial\sigma_{xz}}{\partial x}\frac{h_{\mathrm{b}}}{2}=\int_{-h_{\mathrm{b}}/2}^{h_{\mathrm{b}}/2}\rho_{\mathrm{b}}\,\mathrm{d}z\frac{\partial^2 w_{\mathrm{b}}}{\partial t^2}
\end{aligned}\tag{2}$$

where N_{xx} and M_{xx} are the axial force and moment per unit width; h_{t} and h_{b} are the thickness of the top and bottom face sheets, respectively.

Integration of the fourth equation in Eq. (1) and neglecting the dynamic effect of the core material (Frostig et al., 1992) yield,

$$\sigma_{zz}^{\mathrm{c}}=-\tau_{,x}z+\sigma_{zz}^{\mathrm{c}}\ (x,z=0)\tag{3}$$

Using the constitutive law of the core material,

$$\sigma_{zz}^{\mathrm{c}}=E_{\mathrm{c}}\varepsilon_{zz}^{\mathrm{c}}\tag{4}$$

and considering Eq. (3), we obtain

$$w_{\mathrm{c}}=-\tau_{,x}\frac{z^2}{2E_{\mathrm{c}}}+\frac{\sigma_{zz}^{\mathrm{c}}(x,z=0)}{E_{\mathrm{c}}}z+w_{\mathrm{t}}\tag{5}$$

Substituting in the continuity condition across the bottom interface,

$$w_{\mathrm{b}}=-\tau_{,x}\frac{c^2}{2E_{\mathrm{c}}}+\frac{\sigma_{zz}^{\mathrm{c}}(x,z=0)}{E_{\mathrm{c}}}c+w_{\mathrm{t}}\tag{6}$$

we derive,

$$\sigma_{zz}^{\mathrm{c}}(x,z=0)=\frac{(w_{\mathrm{b}}-w_{\mathrm{t}})E_{\mathrm{c}}}{c}+\tau_{,x}\frac{c}{2}\tag{7}$$

Then, based on the shear compatibility equation,

$$\gamma_{xz}=\frac{\partial u_{\mathrm{c}}}{\partial z}+\frac{\partial w_{\mathrm{c}}}{\partial x}=\frac{\tau}{G_{\mathrm{c}}}\tag{8}$$

Integration of Eq. (8) yields,

$$u_{\mathrm{c}}=u_{0\mathrm{t}}-w_{\mathrm{t},x}\frac{h_{\mathrm{t}}}{2}+\frac{\tau z}{G_{\mathrm{c}}}+\tau_{,xx}\frac{z^3}{6E_{\mathrm{c}}}-w_{\mathrm{t},x}z-\int_0^z\frac{\partial\sigma_{zz}^{\mathrm{c}}(x,z=0)}{\partial x}\frac{z}{E_{\mathrm{c}}}\,\mathrm{d}z\tag{9}$$

Considering the continuity condition across the bottom interface for the horizontal displacement, we obtain,

$$bu_{0\mathrm{b}}-bu_{0\mathrm{t}}+w_{\mathrm{t},x}\frac{b(c+h_{\mathrm{t}})}{2}+w_{\mathrm{b},x}\frac{b(c+h_{\mathrm{b}})}{2}+\tau_{,xx}\frac{bc^3}{12E_{\mathrm{c}}}-\tau\frac{bc}{G_{\mathrm{c}}}=0\tag{10}$$

where b is the width of the beam; c is the height of the core material; u_{0b} and u_{0t} are the horizontal displacements of the top and bottom face sheets at their respective neutral axes.

The constitutive equations of the face sheets (including the bending–stretching coupling effects) are,

$$\begin{aligned} N_{xx} &= A_{11}u_{0,x} - B_{11}w_{,xx} \\ M_{xx} &= B_{11}u_{0,x} - D_{11}w_{,xx} \end{aligned} \tag{11}$$

where A_{11}, B_{11}, and D_{11} are the extensional, extensional–bending coupling, and bending stiffness of the face sheet laminate, respectively.

Further, consider the top and bottom face sheet boundary conditions,

$$\begin{aligned} &\sigma^{t}_{xz}(x, z = -h_t/2) = 0, \quad \sigma^{t}_{xz}(x, z = h_t/2) = \tau, \quad \sigma^{t}_{zz}(x, z = -h_t/2) = -q_t, \\ &\sigma^{t}_{zz}(x, z = h_t/2) = \sigma^{c}_{zz}(x, z = 0), \quad \sigma^{b}_{xz}(x, z = -h_b/2) = \tau, \quad \sigma^{b}_{xz}(x, z = h_b/2) = 0, \\ &\sigma^{b}_{zz}(x, z = -h_b/2) = \sigma^{c}_{zz}(x, z = c), \quad \sigma^{b}_{zz}(x, z = h_b/2) = 0 \end{aligned} \tag{12}$$

where q_t is the external load acting on the top face sheet.

Finally, the governing equations for the dynamic behavior of sandwich beams according to the higher-order theory, in which the dynamic effect of the core is neglected (Model A), are summarized as

$$\begin{aligned} &bB_{11t}u_{0t,xxx} - bD_{11t}w_{t,xxxx} + (w_b - w_t)E_c\frac{b}{c} + \tau_{,x}(c + h_t)\frac{b}{2} = -q_t b + \rho_f h_t b\ddot{w}_t \\ &bA_{11t}u_{0t,xx} - bB_{11t}w_{t,xxx} + b\tau = 0 \\ &bB_{11b}u_{0b,xxx} - bD_{11b}w_{b,xxxx} - (w_b - w_t)E_c\frac{b}{c} + \tau_{,x}(c + h_b)\frac{b}{2} = \rho_b h_b b\ddot{w}_b \\ &bA_{11b}u_{0b,xx} - bB_{11b}w_{b,xxx} - b\tau = 0 \\ &bu_{0b} - bu_{0t} + w_{t,x}\frac{b(c + h_t)}{2} + w_{b,x}\frac{b(c + h_b)}{2} + \tau_{,xx}\frac{bc^3}{12E_c} - \tau\frac{bc}{G_c} = 0 \end{aligned} \tag{13}$$

2.1.2. Model B: Including the partial dynamic effect of the core

If the density of the core can not be neglected, the dynamic effect of the core material should be included. However, the horizontal vibration and rotatory inertia of the core and the face sheets are still not taken into consideration. Integrating the fourth equation in Eq. (1) results in,

$$\sigma^{c}_{zz}(x, z) = \int_0^z \rho_c \frac{\partial^2 w_c}{\partial t^2}\,dz - \int_0^z \tau_{,x}\,dz + \sigma^{c}_{zz}\ (x, z = 0) \tag{14}$$

Using the assumption that the acceleration of the core can be approximated by a linear interpolation of the top face sheet and the bottom face sheet accelerations (Frostig and Baruch, 1994), we have

$$\ddot{w}_c(x, z, t) = \frac{(\ddot{w}_b - \ddot{w}_t)}{c}z + \ddot{w}_t \tag{15}$$

The displacements of the top and bottom face sheets are very close at any transient time; therefore, a linear approximation in Eq. (15) could be a good approximation.

Integration of Eq. (14) results in,

$$\sigma^{c}_{zz} = \frac{\ddot{w}_b - \ddot{w}_t}{c}\frac{\rho_c z^2}{2} + \rho_c z\ddot{w}_t - \tau_{,x}z + \sigma^{c}_{zz}\ (x, z = 0) \tag{16}$$

From the constitutive law of the core material (see Eq. (4)) and satisfying the continuity for the bottom interface, the following compatibility condition is obtained

$$w_t + \frac{\ddot{w}_b - \ddot{w}_t}{E_c}\frac{\rho_c c^2}{6} + \frac{\rho_c c^2}{2E_c}\ddot{w}_t - \frac{\tau_{,x}}{E_c}\frac{c^2}{2} + \frac{\sigma^c(x, z=0)}{E_c}c = w_b \tag{17}$$

Further, solving for the stresses inside the core in terms of w_t, w_b and τ yields

$$\begin{aligned}
\sigma^c_{zz}(x, z=0) &= \frac{(w_b - w_t)E_c}{c} - \frac{(\ddot{w}_b - \ddot{w}_t)}{6}\rho_c c - \frac{1}{2}\rho_c \ddot{w}_t c + \tau_{,x}\frac{c}{2} \\
\sigma^c_{zz}(x, z=c) &= \frac{(w_b - w_t)E_c}{c} + \frac{(\ddot{w}_b - \ddot{w}_t)}{3}\rho_c c + \frac{1}{2}\rho_c \ddot{w}_t c - \tau_{,x}\frac{c}{2} \\
bu_{0b} - bu_{0t} &+ w_{t,x}\frac{b(c+h_t)}{2} + w_{b,x}\frac{b(c+h_b)}{2} + \tau_{,xx}\frac{bc^3}{12E_c} - \tau\frac{bc}{G_c} = 0
\end{aligned} \tag{18}$$

Then the governing equations for the dynamic behavior of sandwich beams according to the higher-order formulation, in which the partial dynamic effect of the core is considered (Model B), are summarized as,

$$\begin{aligned}
&bB_{11t}u_{0t,xxx} - bD_{11t}w_{t,xxxx} + (w_b - w_t)E_c\frac{b}{c} + \tau_{,x}(c+h_t)\frac{b}{2} \\
&\quad = -q_t b + \rho_t h_t b\ddot{w}_t + \rho_c cb\frac{(\ddot{w}_b - \ddot{w}_t)}{6} + \frac{1}{2}\rho_c bc\ddot{w}_t \\
&bA_{11t}u_{0t,xx} - bB_{11t}w_{t,xxx} + b\tau = 0 \\
&bB_{11b}u_{0b,xxx} - bD_{11b}w_{b,xxxx} - (w_b - w_t)E_c\frac{b}{c} + \tau_{,x}(c+h_b)\frac{b}{2} \\
&\quad = \rho_b h_b b\ddot{w}_b + \frac{\ddot{w}_b - \ddot{w}_t}{3}\rho_c cb + \frac{1}{2}\rho_c cb\ddot{w}_t \\
&bA_{11b}u_{0b,xx} - bB_{11b}w_{b,xxx} - b\tau = 0 \\
&bu_{0b} - bu_{0t} + w_{t,x}\frac{b(c+h_t)}{2} + w_{b,x}\frac{b(c+h_b)}{2} + \tau_{,xx}\frac{bc^3}{12E_c} - \tau\frac{bc}{G_c} = 0
\end{aligned} \tag{19}$$

2.1.3. Model C: With the full dynamic effect of the core

In Model C, the full dynamic effect (i.e., besides the mass inertia of the core, both the horizontal vibration and rotatory inertia of the core are also included) is considered in the analysis. By using the equilibrium condition given in Eq. (1) and assuming that the in-plane stress of the core is relatively small (in this study, it is assumed to be zero) and that the shear stress is constant over the thickness of the core, the horizontal and vertical accelerations of the core can be approximated by a linear interpolation from those of face sheets (Frostig and Baruch, 1994) as

$$\begin{aligned}
\ddot{u}_c(x, z, t) &= \frac{(\ddot{u}_b - \ddot{u}_t)}{c}z + \ddot{u}_t \\
\ddot{w}_c(x, z, t) &= \frac{(\ddot{w}_b - \ddot{w}_t)}{c}z + \ddot{w}_t
\end{aligned} \tag{20}$$

where u_t, u_b, w_t and w_b are the top and bottom interface horizontal displacements and the top and bottom interface vertical displacement, respectively.

Integrating the third equation in Eq. (1) and considering that the in-plane stresses do not exist in the core and the shear stress τ does not change over the height, we have

$$\int_0^c \rho_c \ddot{u}_c(x,z,t)\,dz = 0 \tag{21}$$

Substituting $\ddot{u}_c(x,z,t) = \frac{\ddot{u}_c^{bot} - \ddot{u}_c^{top}}{c} z + \ddot{u}_c^{top}$ into Eq. (21), we derive,

$$\begin{aligned} &\ddot{u}_c^{bot} = -\ddot{u}_c^{top} \\ &\ddot{u}_{0b} + \frac{1}{2}h_b\frac{\partial \ddot{w}_b}{\partial x} = -\ddot{u}_{0t} + \frac{1}{2}h_t\frac{\partial \ddot{w}_t}{\partial x} \end{aligned} \tag{22}$$

From the fourth equation of Eq. (1),

$$\sigma_{zz}^c = \frac{\ddot{w}_b - \ddot{w}_t}{c}\frac{\rho_c z^2}{2} + \rho_c z\ddot{w}_t - \tau_{,x} z + \sigma_{zz}^c \ (x, z=0) \tag{23}$$

Using the constitutive law of the core material in Eq. (4) and satisfying the continuity conditions for the bottom interface, we have

$$w_c = w_t + \frac{\ddot{w}_b - \ddot{w}_t}{E_c c}\frac{\rho_c z^3}{6} + \frac{\rho_c z^2}{2E_c}\ddot{w}_t - \frac{\tau_{,x}}{E_c}\frac{z^2}{2} + \frac{\sigma^c(x,z=0)}{E_c} z \tag{24}$$

$$\sigma_{zz}^c(x,z=0) = \frac{(w_b - w_t)E_c}{c} - \frac{(\ddot{w}_b - \ddot{w}_t)}{6}\rho_c c - \frac{1}{2}\rho_c \ddot{w}_t c + \tau_{,x}\frac{c}{2} \tag{25}$$

Further, considering the continuity of the horizontal displacements across the bottom interface,

$$\gamma_{xz} = \frac{\partial u_c}{\partial z} + \frac{\partial w_c}{\partial x} = \frac{\tau}{G_c} \tag{26}$$

$$\frac{\partial u_c}{\partial z} = \frac{\tau}{G_c} - \frac{\partial w_c}{\partial x} \tag{27}$$

and integrating Eq. (27), we obtain

$$\begin{aligned} u_c = {} & \frac{\tau z}{G_c} + u_{0t} - w_{t,x}\frac{h_t}{2} - \int_0^z \frac{\partial(\ddot{w}_b - \ddot{w}_t)}{\partial x}\frac{\rho_c z^3}{6E_c c}\,dz - \frac{1}{2}\int_0^z \frac{\rho_c z^2}{E_c}\frac{\partial \ddot{w}_t}{\partial x}\,dz + \int_0^z \tau_{,xx}\frac{z^2}{2E_c}\,dz \\ & - \int_0^z \frac{\sigma_{zz,x}^c(x,z=0)}{E_c} z\,dz - \int_0^z \frac{\partial w_t}{\partial x}\,dz \end{aligned} \tag{28}$$

where γ_{xz} is the shear strain in the core.

Satisfying the displacement continuity across the interface of the core and the bottom face sheet, we have,

$$\begin{aligned} u_{0b} + \frac{h_b}{2}w_{b,x} = {} & \frac{\tau c}{G_c} + u_{0t} - w_{t,x}\frac{h_t}{2} - \int_0^c \frac{\partial(\ddot{w}_b - \ddot{w}_t)}{\partial x}\frac{\rho_c z^3}{6E_c c}\,dz - \frac{1}{2}\int_0^c \frac{\rho_c z^2}{E_c}\frac{\partial \ddot{w}_t}{\partial x}\,dz + \int_0^c \tau_{,xx}\frac{z^2}{2E_c}\,dz \\ & - \int_0^c \frac{\sigma_{zz,x}^c(x,z=0)}{E_c} z\,dz - \int_0^c \frac{\partial w_t}{\partial x}\,dz \end{aligned} \tag{29}$$

$$bu_{0b} - bu_{0t} + w_{t,x}\frac{b(c+h_t)}{2} + w_{b,x}\frac{b(c+h_b)}{2} + \tau_{,xx}\frac{bc^3}{12E_c} - \tau\frac{bc}{G_c} = \frac{\rho_c bc^3}{24E_c}\left(\frac{\partial \ddot{w}_b}{\partial x} - \frac{\partial \ddot{w}_t}{\partial x}\right) + \frac{\rho_c bc^3}{12E_c}\frac{\partial \ddot{w}_t}{\partial x} \tag{30}$$

Finally, the governing equations for the dynamic behavior of soft-core sandwich beams according to the higher order theory and with full consideration of dynamic effect of the core (Model C), are summarized as,

$$\begin{aligned}
&bB_{11t}u_{0t,xxx} - bD_{11t}w_{t,xxxx} + (w_b - w_t)E_c\frac{b}{c} + \tau_{,x}(c+h_t)\frac{b}{2} \\
&\quad = -q_t b + \rho_f h_t b\ddot{w}_t + \rho_c cb\frac{(\ddot{w}_b - \ddot{w}_t)}{6} + \frac{1}{2}\rho_c cb\ddot{w}_t \\
&bA_{11t}u_{0t,xx} - bB_{11t}w_{t,xxx} + b\tau = \rho_t h_t b\ddot{u}_{0t} \\
&bB_{11b}u_{0b,xxx} - bD_{11b}w_{b,xxxx} - (w_b - w_t)E_c\frac{b}{c} + \tau_{,x}(c+h_b)\frac{b}{2} \\
&\quad = \rho_b h_b b\frac{\partial^2 w_b}{\partial t^2} + \frac{\ddot{w}_b - \ddot{w}_t}{3}\rho_c cb + \frac{1}{2}\rho_c cb\ddot{w}_t \\
&bA_{11b}u_{0b,xx} - bB_{11b}w_{b,xxx} - b\tau = \rho_b h_b b\ddot{u}_{0b} \\
&bu_{0b} - bu_{0t} + w_{t,x}\frac{b(c+h_t)}{2} + w_{b,x}\frac{b(c+h_b)}{2} + \tau_{,xx}\frac{bc^3}{12E_c} - \tau\frac{bc}{G_c} \\
&\quad = \frac{\rho_c bc^3}{24E_c}\frac{\partial\ddot{w}_b}{\partial x} + \frac{\rho_c bc^3}{24E_c}\frac{\partial\ddot{w}_t}{\partial x}
\end{aligned} \tag{31}$$

2.2. Dynamics of the projectile

2.2.1. Point load—effect of concentrated force

In this study, it is assumed that the vibration of the projectile can be neglected. The Hertzian contact law (Abrate, 1997) is adopted,

$$F(t) = K_c\alpha^{3/2} \tag{32}$$

where α is the relative indentation between the projectile and the plate, and K_c is the Hertzian contact stiffness defined by,

$$K_c = \frac{4}{3}E_{22}\sqrt{R} \tag{33}$$

where E_{22} is the transverse Young's modulus of the face sheet and R is the radius of the projectile tip. In Eq. (33), E_{33} should be used instead of E_{22}. However, for the general composites (e.g., unidirectional composites), E_{33} is equal or close to E_{22}. Thus, as an approximation, E_{22} is used in this study.

The relative indentation α is defined as,

$$\alpha = w_p - w_t\left(\frac{a}{2}, -\frac{h_t}{2}\right) \tag{34}$$

where w_p denotes the displacement of projectile, and $w(a/2, -h_t/2)$ is the transverse displacement of the top face sheet at the impact location. In this study, α can be a distributed indentation according to the shape of projectile tip (Yang and Qiao, 2005).

Then the equation of motion for the projectile can be written as,

$$m\ddot{w}_p + F(t) = 0, \quad w_p = 0, \quad \dot{w}_p = v_0 \tag{35}$$

where m is the mass of the projectile, w_p is the displacement of the projectile, and $F(t)$ is the contact force between the projectile and the sandwich panel.

2.2.2. Patch load—effect of distributed force

Based on Herztian contact stress distribution, a distributed load like a parabolic function is assumed,

$$q(x,t) = P_0(t)\left(1 - \frac{(x-x_0)^2}{a(t)^2}\right)^{1/2} \tag{36}$$

where x_0 is the coordinate of the first contact point, $P_0(t)$ is the maximal value of the distribution, $q(x,t)$ is the distributed force generated by a foreign object impact.

The contact force p is accounted for by solving Hertz's problem, and given as

$$p = k\alpha^{3/2} \tag{37}$$

where $k = \left(\frac{9}{256}\frac{(\theta_1+\theta)^2}{R}\right)^{-1/2}$, $\theta_1 = \frac{4(1-\mu_1^2)}{E_1}$, $\theta = \frac{4(1-\mu^2)}{E}$, E, μ are the Young's modulus and Poisson's ratio of the indenter material, and E_1, μ_1 are the similar material properties of the first top layer of the face sheet laminate, p is the resultant contact force.

Then, $P_0(t)$ can be solved by integrating the above equation,

$$P_0(t) = \frac{3}{4}\frac{p}{a(t)\times b} \tag{38}$$

where $a(t) = \sqrt{\alpha(2R-\alpha)}$, $a(t)$ is the contact radius.

2.3. Sandwich beams under simply supported boundary condition over impact

In this study, a sandwich beam with simply supported boundary conditions is considered, and the Rayleigh–Ritz method is used to solve the proposed models A to C as given in Section 2.1.

Assume the shape functions for displacement and shear stress as

$$\begin{aligned}
w_t(x,t) &= C_t(t)\sin\left(\frac{n\pi x}{L}\right)\\
w_b(x,t) &= C_b(t)\sin\left(\frac{n\pi x}{L}\right)\\
u_{0t}(x,t) &= C_{ut}(t)\cos\left(\frac{n\pi x}{L}\right)\\
u_{0b}(x,t) &= C_{ub}(t)\cos\left(\frac{n\pi x}{L}\right)\\
\tau(x,t) &= C_\tau(t)\cos\left(\frac{n\pi x}{L}\right)
\end{aligned} \tag{39}$$

where $C_t(t)$, $C_b(t)$, $C_{ut}(t)$, $C_{ub}(t)$, and $C_\tau(t)$ are the amplitude for each vibration mode.

The external force can be assumed as

$$F(x,t) = Q(t)\sin\left(\frac{n\pi x}{L}\right) \tag{40}$$

where $Q(t)$ is the forcing component for each vibration mode. Then, the governing equations for the aforementioned models (A to C) are obtained as follows.

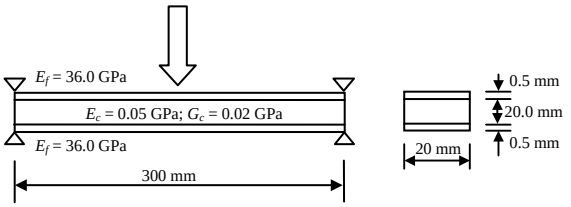

Fig. 2. The physical model of a sandwich beam.

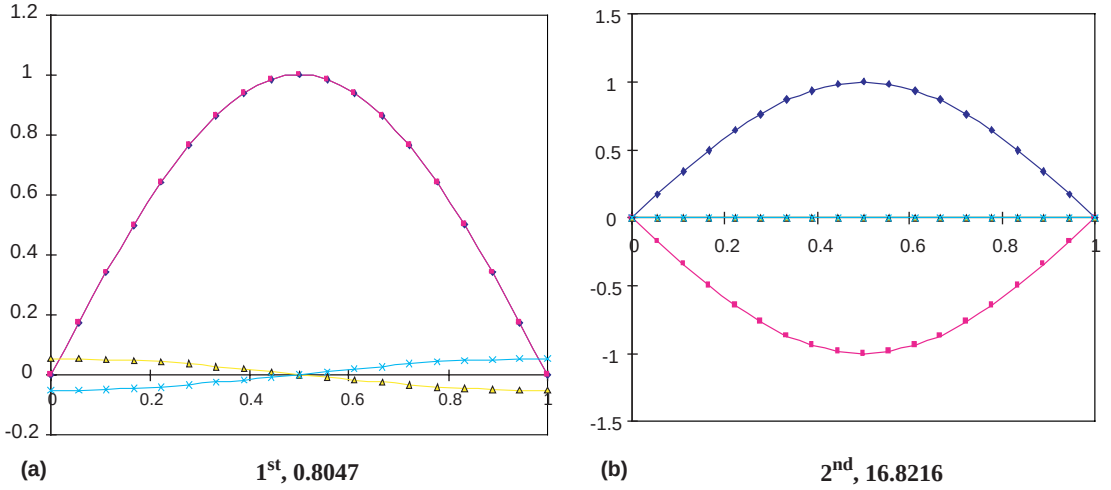

Fig. 3. Eigenmodes of the symmetrical sandwich beam with $n = 1$ (Model A): Mode number and dimensionless frequency ((♦) w_t, (■) w_b, (▲) u_t, (-×-) u_b).

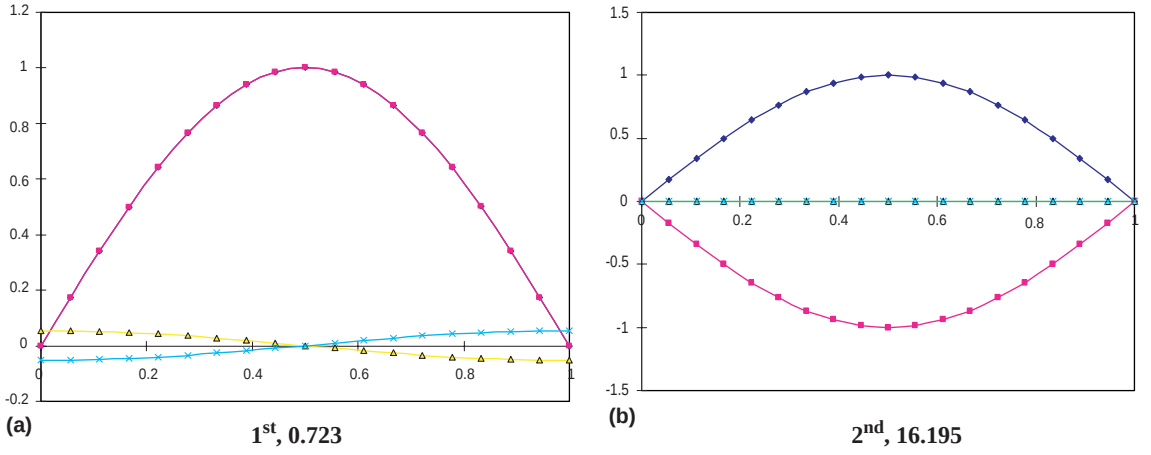

Fig. 4. Eigenmodes of the symmetrical sandwich beam with $n = 1$ (Model B): Mode number and dimensionless frequency ((♦) w_t, (■) w_b, (▲) u_t, (-×-) u_b).

2.3.1. Governing equations for Model A

The governing equations for Model A, in which the dynamic effect of the core is neglected, can be written in the matrix form as,

$$\begin{bmatrix} P_{11} & P_{12} & 0 & 0 & 0 \\ P_{12} & P_{22} & 0 & 0 & 0 \\ 0 & 0 & 0 & 0 & 0 \\ 0 & 0 & 0 & 0 & 0 \\ 0 & 0 & 0 & 0 & 0 \end{bmatrix} \begin{bmatrix} \ddot{C}_{\mathrm{t}}(t) \\ \ddot{C}_{\mathrm{b}}(t) \\ \ddot{C}_{\mathrm{ut}}(t) \\ \ddot{C}_{\mathrm{ub}}(t) \\ \ddot{C}_{\tau}(t) \end{bmatrix} + \begin{bmatrix} F_{11} & F_{12} & F_{13} & 0 & F_{15} \\ F_{12} & F_{22} & 0 & F_{24} & F_{25} \\ F_{13} & 0 & F_{33} & 0 & F_{35} \\ 0 & F_{24} & 0 & F_{44} & F_{45} \\ F_{15} & F_{25} & F_{35} & F_{45} & F_{55} \end{bmatrix} \begin{bmatrix} C_{\mathrm{t}}(t) \\ C_{\mathrm{b}}(t) \\ C_{\mathrm{ut}}(t) \\ C_{\mathrm{ub}}(t) \\ C_{\tau}(t) \end{bmatrix} = \begin{bmatrix} -Q(t) \\ 0 \\ 0 \\ 0 \\ 0 \end{bmatrix} \tag{41}$$

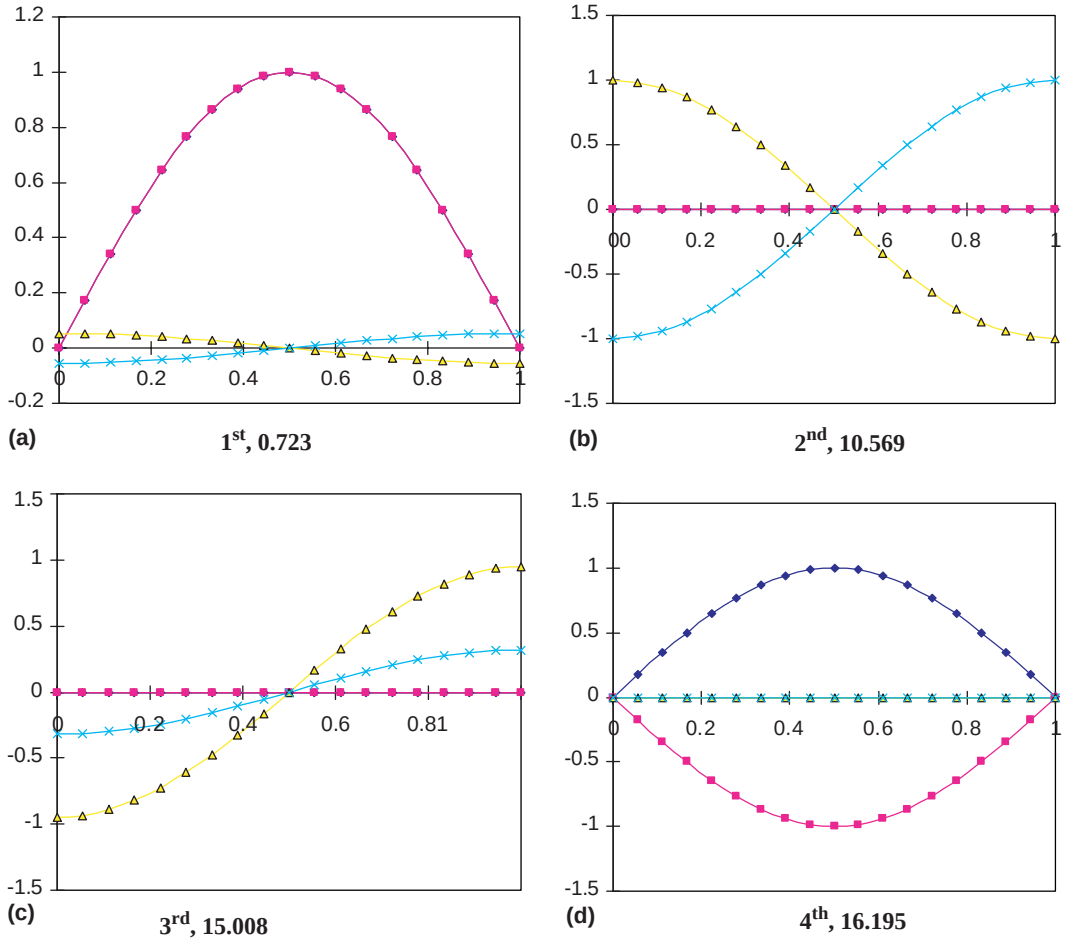

Fig. 5. Eigenmodes of the symmetrical sandwich beam with $n = 1$ (Model C): Mode number and dimensionless frequency ((♦) w_{t}, (■) w_{b}, (▲) u_{t}, (–×–) u_{b}).

Table 1
Comparison of frequencies of the proposed three models with the results from the finite element analysis by ABAQUS and Frostig and Baruch (1994)'s model

Wave no.	Model A	Model B	Model C	Frostig and Baruch (1994)	ABAQUS
$n=1$	362.96/7587.43	326.39/7304.78	325.98/4767.31/6769.24/7304.79	325.98/4287.00/6518.11/7304.78	349.86
$n=2$	918.50/7587.47	825.96/7304.85	824.96/7304.85/9534.62/10674.70	825.30/7304.80/8574.00/10278.70	777.42
$n=3$	1457.84/7587.70	1301.96/7305.05	1308.90/7305.05/14301.90/15080.00	1310.38/7305.01/12861.00/14520.40	1221.21
$n=4$	1979.78/7588.28	1780.31/7305.53	1776.11/7305.63/19069.30/19652.80	1779.83/7305.53/17148.00/18923.40	1657.33
$n=5$	2488.07/7589.56	2237.38/7306.85	2229.62/7306.85/23836.60/24299.00	2237.02/7306.71/21435.00/23396.70	2089.55

where

$$F_{11}=\frac{bE_c}{c}+\frac{bD_{11t}n^4\pi^4}{L^4},\quad F_{12}=-\frac{bE_c}{c},\quad F_{13}=-\frac{bB_{11t}n^3\pi^3}{L^3},\quad F_{14}=0$$

$$F_{15}=\frac{bcn\pi}{2L}+\frac{bd_tn\pi}{2L},\quad F_{22}=\frac{bE_c}{c}+\frac{bD_{11b}n^4\pi^4}{L^4},\quad F_{24}=-\frac{bB_{11b}n^3\pi^3}{L^3}$$

$$F_{25}=\frac{bcn\pi}{2L}+\frac{bd_bn\pi}{2L},\quad F_{33}=\frac{bA_{11t}n^2\pi^2}{L^2},\quad F_{35}=-b,\quad F_{44}=\frac{bA_{11b}n^2\pi^2}{L^2}$$

$$F_{45}=b,\quad F_{55}=-\frac{bc}{G_c}-\frac{bc^3n^2\pi^2}{12E_cL^2},\quad P_{11}=\rho_th_tb,\quad P_{22}=\rho_bh_bb,\quad P_{12}=0$$

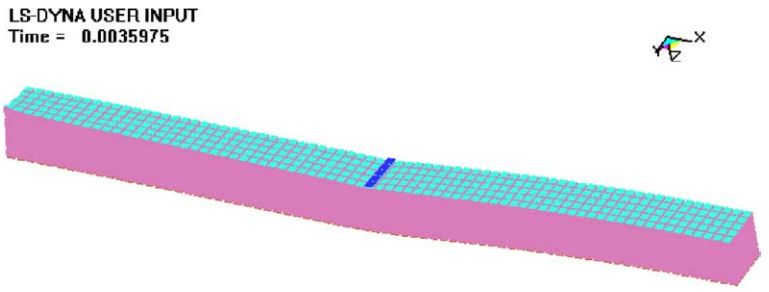

Fig. 6. The LS-DYNA finite element modeling of a sandwich beam.

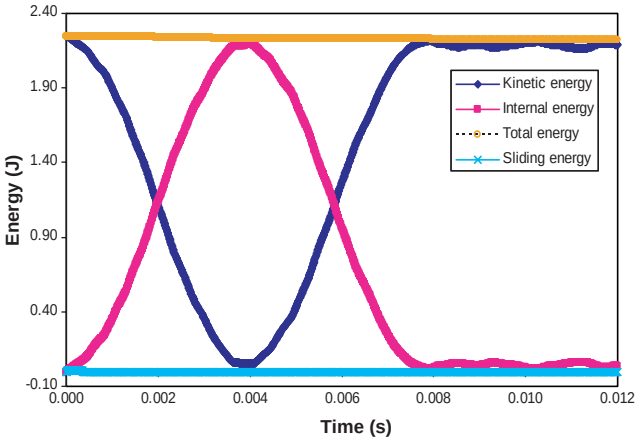

Fig. 7. Energy vs. time history in the LS-DYNA finite element model.

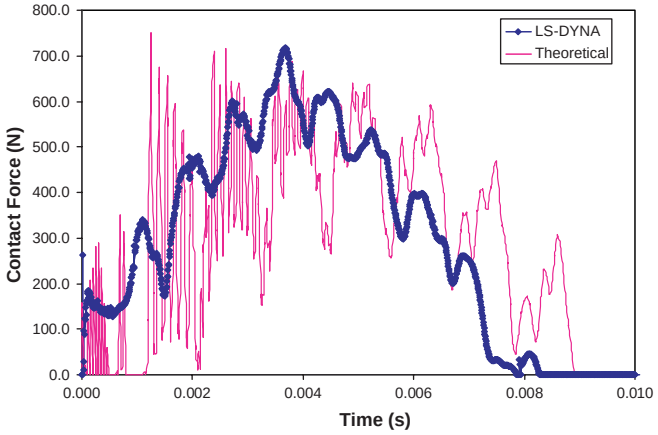

Fig. 8. Comparison of the contact force history.

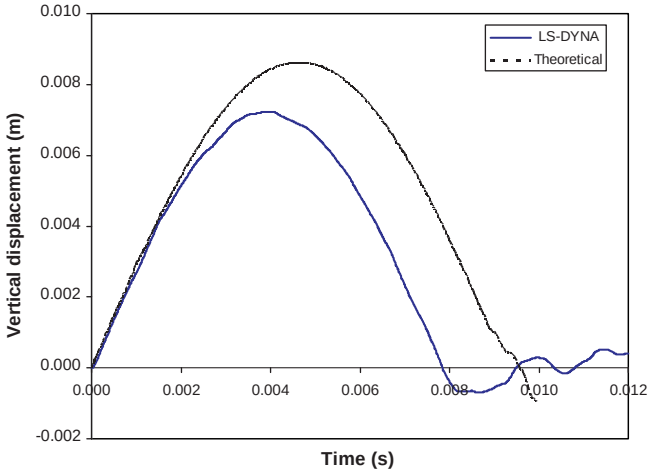

Fig. 9. Comparison of the central deflection history of top face sheet.

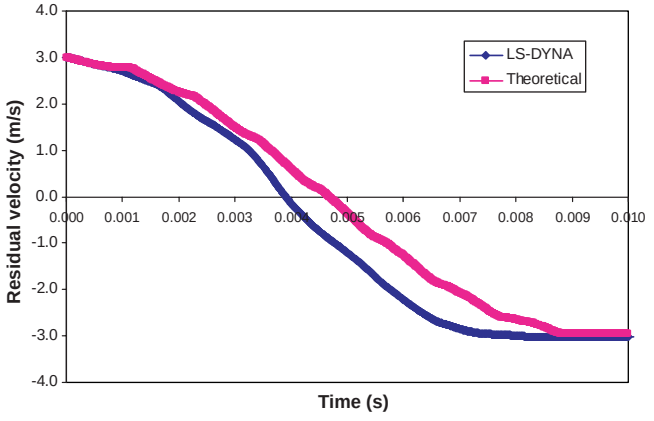

Fig. 10. Comparison of the residual velocity history.

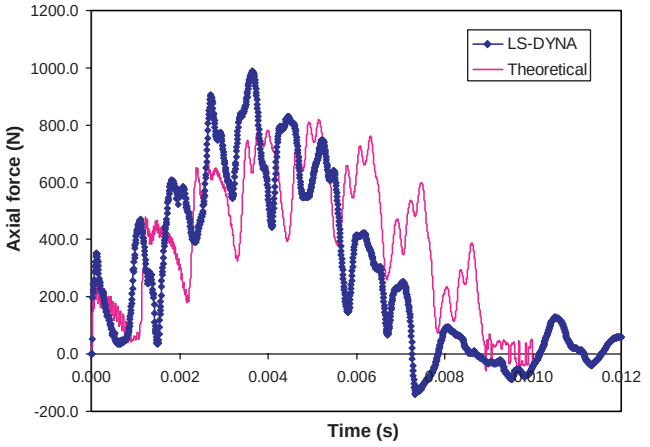

Fig. 11. Comparison of the maximal axial force history.

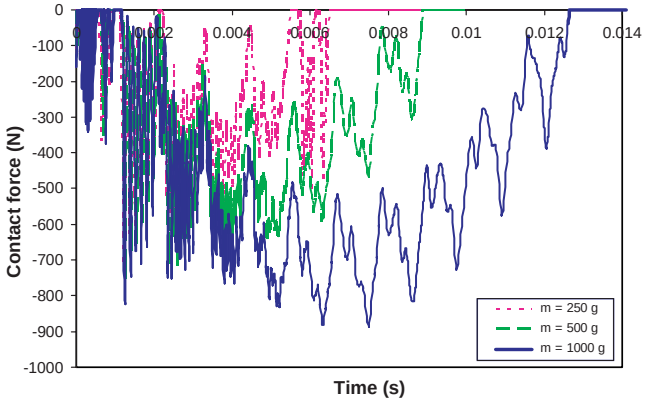

Fig. 12. The contact force history under three different impact masses.

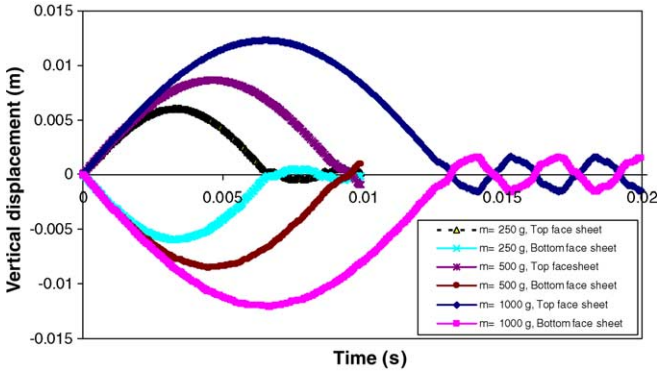

Fig. 13. The central top and bottom face sheet deflection history under three different impact masses.

Reducing the equations using the relationship between the last three rows in the matrix, Eq. (41) was reduced to,

$$\begin{bmatrix} P_{11} & P_{12} \\ P_{12} & P_{22} \end{bmatrix} \begin{bmatrix} \ddot{C}_t(t) \\ \ddot{C}_b(t) \end{bmatrix} + \begin{bmatrix} K_{11} & K_{12} \\ K_{12} & K_{22} \end{bmatrix} \begin{bmatrix} C_t(t) \\ C_b(t) \end{bmatrix} = \begin{bmatrix} -Q(t) \\ 0 \end{bmatrix} \tag{42}$$

where

$$K_{11} = F_{11} + \frac{-F_{15}^2 F_{33} F_{44} + 2F_{13} F_{15} F_{35} F_{44} + F_{13}^2 F_{45}^2 - F_{13}^2 F_{44} F_{45}}{F_{33} F_{44} F_{55} - F_{35}^2 F_{44} - F_{33} F_{45}^2}$$

$$K_{12} = F_{12} + \frac{-F_{15} F_{25} F_{33} F_{44} + F_{13} F_{25} F_{35} F_{44} + F_{15} F_{24} F_{33} F_{45} - F_{13} F_{24} F_{35} F_{45}}{F_{33} F_{44} F_{55} - F_{35}^2 F_{44} - F_{33} F_{45}^2}$$

$$K_{22} = F_{22} + \frac{F_{24}^2 F_{35}^2 - F_{25}^2 F_{33} F_{44} + 2F_{24} F_{25} F_{33} F_{45} - F_{24}^2 F_{33} F_{55}}{F_{33} F_{44} F_{55} - F_{35}^2 F_{44} - F_{33} F_{45}^2}$$

By combining Eq. (42) with the equation of motion of the projectile,

$$m\ddot{w}_p + F(x,t) = 0 \tag{43}$$

the governing equations can be established.

The equations (Eqs. (42) and (43)) can be solved simultaneously, and the corresponding transient response and other terms, like the transverse normal stresses over the interfaces, bending moments, and axial forces in the two face sheets as well as the deformation pattern in the core can be obtained.

2.3.2. Governing equations for Model B

Similarly, the governing equations for Model B, in which the partial dynamic effect of the core is included, can be written in the matrix form as,

$$\begin{bmatrix} P'_{11} & P'_{12} \\ P'_{12} & P'_{22} \end{bmatrix} \begin{bmatrix} \ddot{C}_t(t) \\ \ddot{C}_b(t) \end{bmatrix} + \begin{bmatrix} K_{11} & K_{12} \\ K_{12} & K_{22} \end{bmatrix} \begin{bmatrix} C_t(t) \\ C_b(t) \end{bmatrix} = \begin{bmatrix} -Q(t) \\ 0 \end{bmatrix} \tag{44}$$

where $P'_{11} = \rho_t h_t b + \frac{1}{3}\rho_c cb,\ P'_{12} = \frac{1}{6}\rho_c cb,\ P'_{22} = \rho_b h_b b + \frac{1}{3}\rho_c cb.$

2.3.3. Governing equations for Model C

Finally, the governing equations for Model C, in which the dynamic effect of the core is fully considered, is given as

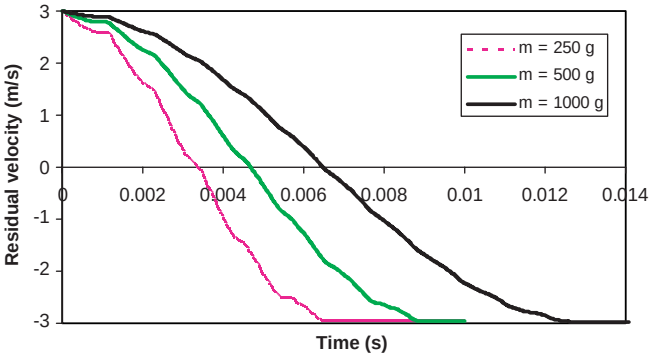

Fig. 14. The residual velocity history under three different impact masses.

$$\begin{bmatrix} P'_{11} & P'_{12} & 0 & 0 & 0 \\ P'_{12} & P'_{22} & 0 & 0 & 0 \\ 0 & 0 & P'_{33} & 0 & 0 \\ 0 & 0 & 0 & P'_{44} & 0 \\ P'_{51} & P'_{52} & 0 & 0 & 0 \end{bmatrix} \begin{bmatrix} \ddot{C}_{\mathrm{t}}(t) \\ \ddot{C}_{\mathrm{b}}(t) \\ \ddot{C}_{\mathrm{ut}}(t) \\ \ddot{C}_{\mathrm{ub}}(t) \\ \ddot{C}_{\tau}(t) \end{bmatrix} + \begin{bmatrix} F_{11} & F_{12} & F_{13} & 0 & F_{15} \\ F_{12} & F_{22} & 0 & F_{24} & F_{25} \\ F_{13} & 0 & F_{33} & 0 & F_{35} \\ 0 & F_{24} & 0 & F_{44} & F_{45} \\ F_{15} & F_{25} & F_{35} & F_{45} & F_{55} \end{bmatrix} \begin{bmatrix} C_{\mathrm{t}}(t) \\ C_{\mathrm{b}}(t) \\ C_{\mathrm{ut}}(t) \\ C_{\mathrm{ub}}(t) \\ C_{\tau}(t) \end{bmatrix} = \begin{bmatrix} -Q(t) \\ 0 \\ 0 \\ 0 \\ 0 \end{bmatrix} \tag{45}$$

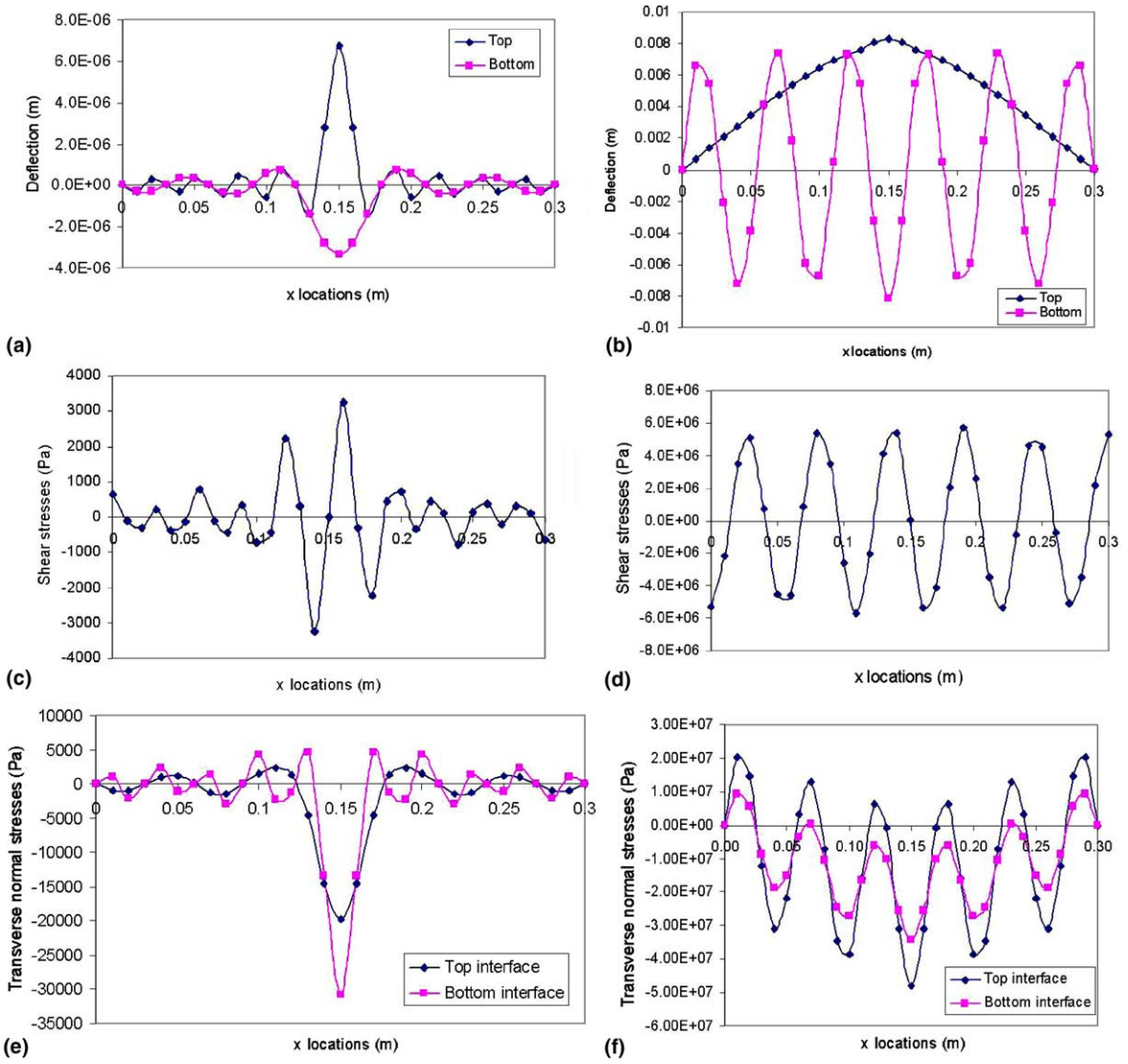

Fig. 15. The various stress generated and the core compression produced in the case of $m = 500$ g and $V_0 = 3.0$ m/s. Deflection distribution of the top and bottom face sheets at: (a) $t = 1.0 \times 10^{-5}$ s and (b) $t = 5.44 \times 10^{-3}$ s. Shear stress distribution in the core at: (c) $t = 1.0 \times 10^{-5}$ s and (d) $t = 5.44 \times 10^{-3}$ s. Transverse normal stress distribution at the two interfaces at: (e) $t = 1.0 \times 10^{-5}$ s and (f) $t = 5.44 \times 10^{-3}$ s. Axial stress distribution at the two face sheets at: (g) $t = 1.0 \times 10^{-5}$ s and (h) $t = 5.44 \times 10^{-3}$ s. Vertical displacement distribution in the core at: (i) $t = 1.0 \times 10^{-5}$ s and (j) $t = 5.44 \times 10^{-3}$ s.

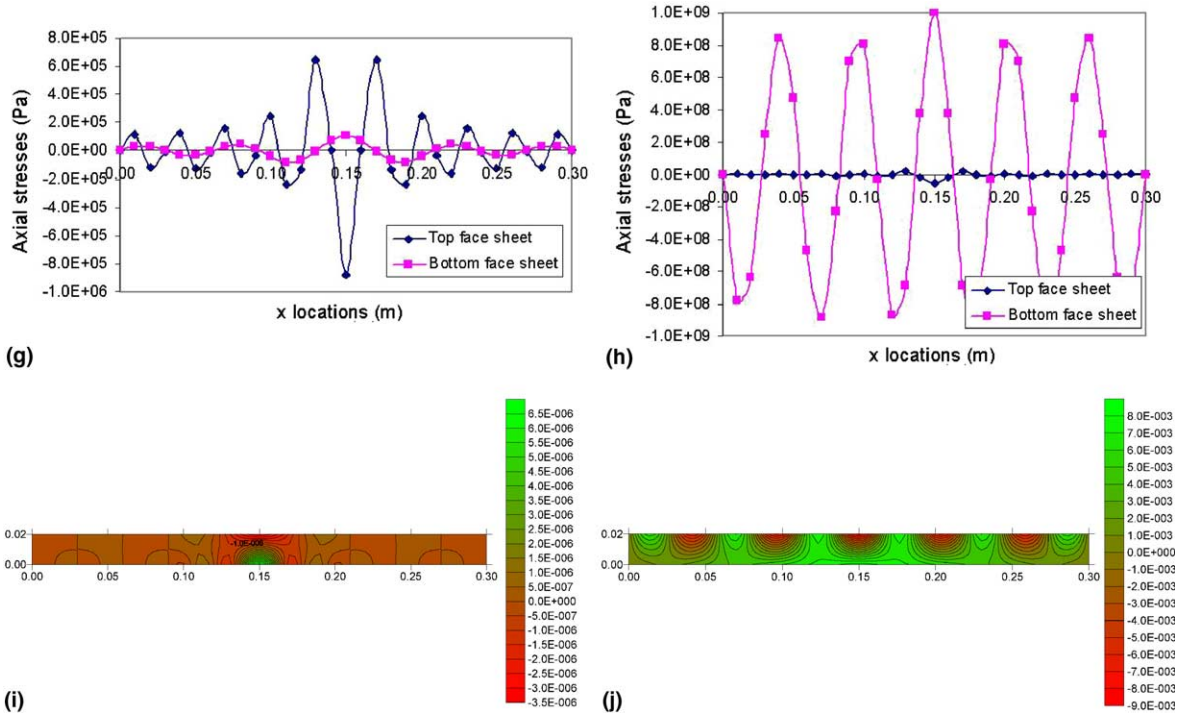

Fig. 15 (*continued*)

where $P'_{11} = \rho_t h_t b + \frac{1}{3}\rho_c cb$, $P'_{12} = \frac{1}{6}\rho_c cb$, $P'_{22} = \rho_b h_b b + \frac{1}{3}\rho_c cb$, $P'_{33} = \rho_t h_t b$, $P'_{44} = \rho_b h_b b$, $P'_{51} = \frac{\rho_c bc^3}{24E_c}\frac{n\pi}{L}$, $P'_{52} = \frac{\rho_c bc^3}{24E_c}\frac{n\pi}{L}$.

2.3.4. Mode summation and solution procedure

In order to approximate the vibrating state of the sandwich beams under impact, the vertical and horizontal displacements of the face sheets as well as the shear stress of the core are represented by mode summation using the normal modes discussed in Eq. (39) as,

$$
\begin{aligned}
w_t(x,t) &= \sum_{n=1}^{N} C_{nt}(t)\sin\left(\frac{n\pi x}{L}\right)\\
w_b(x,t) &= \sum_{n=1}^{N} C_{nb}(t)\sin\left(\frac{n\pi x}{L}\right)\\
w_t(x,t) &= \sum_{n=1}^{N} C_{nut}(t)\sin\left(\frac{n\pi x}{L}\right)\\
u_{0b}(x,t) &= \sum_{n=1}^{N} C_{nub}(t)\cos\left(\frac{n\pi x}{L}\right)\\
\tau(x,t) &= \sum_{n=1}^{N} C_{n\tau}\ (t)\cos\left(\frac{n\pi x}{L}\right)\\
F(x,t) &= \sum_{n=1}^{N} Q_n(t)\sin\left(\frac{n\pi x}{L}\right)
\end{aligned}
\tag{46}
$$

A standard modal analysis can be used, and it yields,

$$\begin{bmatrix} \ddot{C}_{nt}(t) \\ \ddot{C}_{nb}(t) \\ \ddot{C}_{nut}(t) \\ \ddot{C}_{nub}(t) \\ \ddot{C}_{n\tau}(t) \end{bmatrix} + \left[\omega_n^2\right] \begin{bmatrix} C_{nt}(t) \\ C_{nb}(t) \\ C_{nut}(t) \\ C_{nub}(t) \\ C_{n\tau}(t) \end{bmatrix} = \begin{bmatrix} -Q_n(t) \\ 0 \\ 0 \\ 0 \\ 0 \end{bmatrix} \tag{47}$$

where ω_n is the natural frequency for each vibrating mode.

For an N mode approximation, Eq. (47) can be combined with the equation of motion of the projectile (Eq. (43)) and solved by the numerical time integration.

3. Higher-order free vibration analysis

The three aforementioned models (Models A to C) are used to study the free vibration behavior of the sandwich beams, and the validity of the models is demonstrated by comparing with numerical

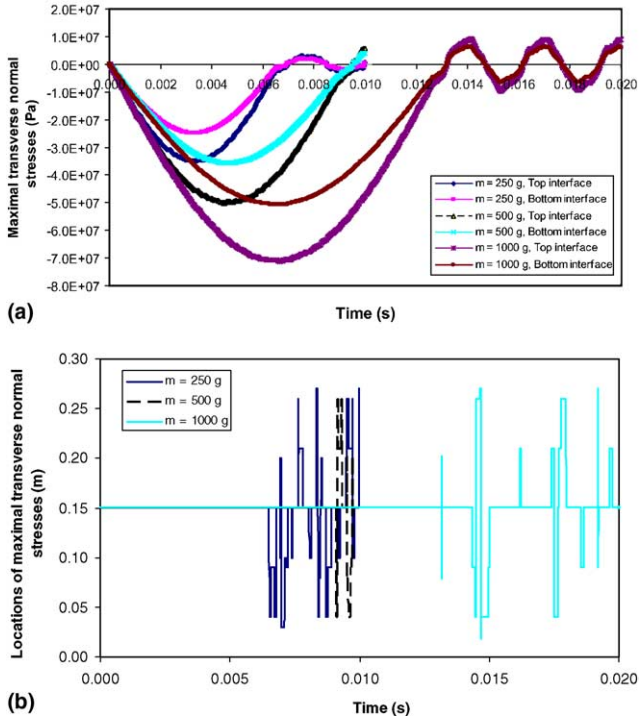

Fig. 16. Maximal transverse normal stresses and their locations at the interfaces under three different impact masses. (a) Maximal transverse normal stresses at the two interfaces. (b) Locations of the maximal transverse normal stresses happened at the top interface.

results obtained from finite element simulations using ABAQUS and the solution by Frostig and Baruch (1994).

The physical model of a sandwich beam is shown in Fig. 2, with the labeled material and geometrical parameters. The mechanical properties of the face sheets correspond to a quasi-isotropic glass-ceramic composite with a density of 4400 kg/m^3; whereas those of the core correspond to an isotropic polymethacrylimide rigid foam with a density of 52.06 kg/m^3. In the later impact analysis (see Section 4), the projectile hits the sandwich beam from the top.

3.1. Natural frequencies and mode shapes

The two eigenmodes corresponding to the first wave number (i.e., $n = 1$) are shown in Fig. 3. The eigenfrequencies are presented in a non-dimensional form relative to the eigenfrequency of 451.053 Hz for an ordinary beam having the same mass and total flexural rigidity. In the first mode ($n = 1$), the anti-symmetric mode, in which the two skins move vertically in the same direction with the same amplitude, corresponds to the lower frequency; while the symmetric mode corresponds to the higher frequency, in which the two skins move vertically in the opposite direction with the same amplitude. Because the vibration of horizontal displacement is neglected, the modes for the horizontal displacements do not exist in Model A.

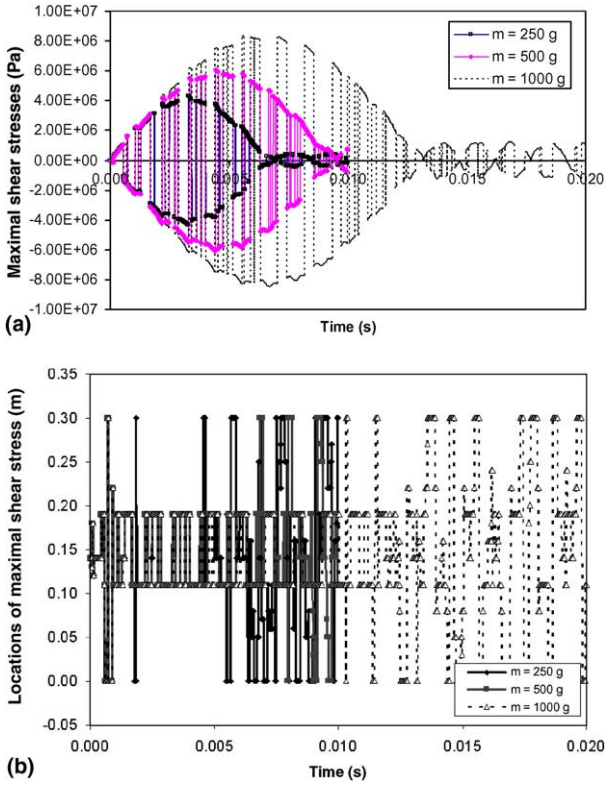

Fig. 17. Maximal shear stresses and their locations in the core under three different impact masses. (a) Maximal shear stresses in the core. (b) Locations of the maximal shear stresses.

The two eigenmodes for Model B corresponding to the first wave number, $n = 1$, are shown in Fig. 4. Similar to the eigenmodes of Model A, the same mode shapes are generated by Model B, but with different natural frequencies. Again, since only the core mass is included in the analysis, the modes for the horizontal displacements do not exist for model B either.

The four eigenmodes for Model C corresponding to the first wave number, $n = 1$, are shown in Fig. 5. Because the vibrations corresponding to horizontal displacements are considered in Model C, the modes for the horizontal displacements are included. Compared with Models A and B, this model captures the whole picture of the vibration of sandwich beams.

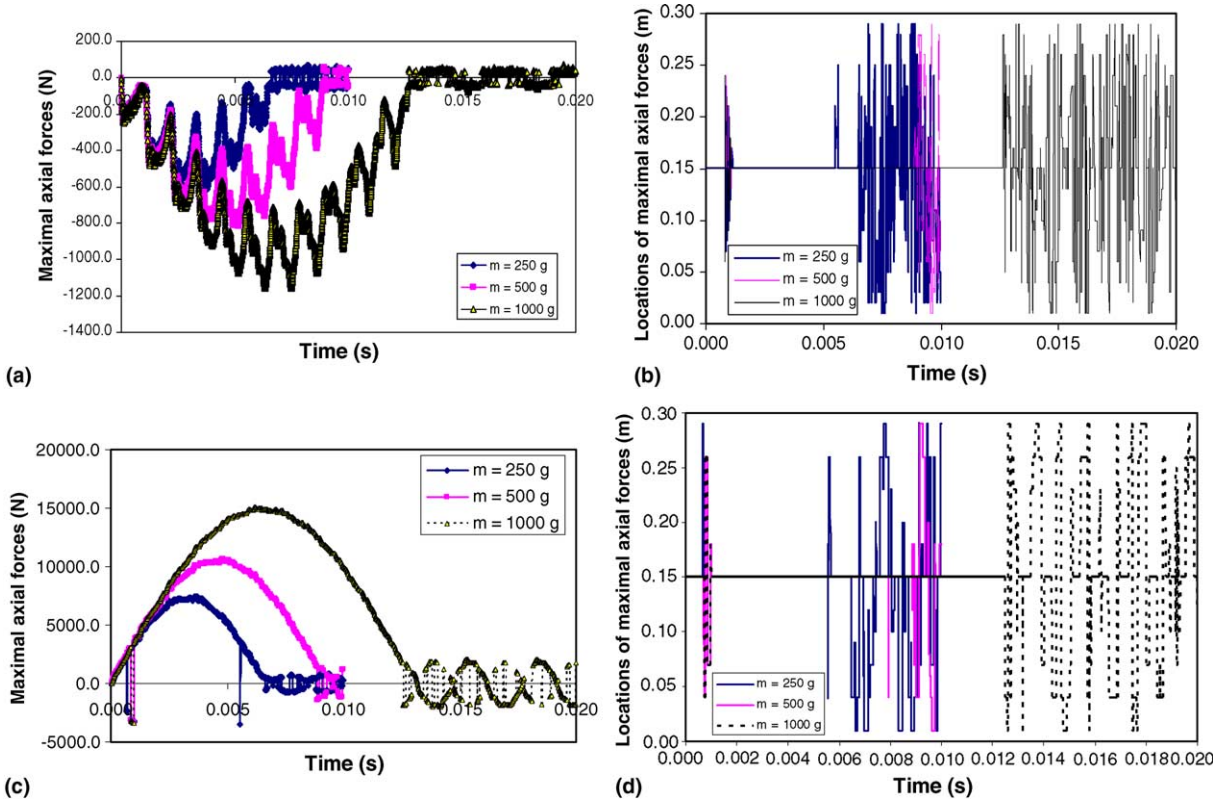

Fig. 18. Maximal axial forces and their locations in the face sheets under three different impact masses. (a) Maximal axial stresses in the top face sheet. (b) Maximal axial stresses locations at each time step in the top face sheet. (c) Maximal axial stress in the bottom face sheet. (d) Maximal axial stress locations at each time step in the bottom face sheet.

Table 2
Quasi-static strength data of a sandwich system with woven roving prepreg face sheet and honeycomb core (Mines et al., 1998)

Strength	$\sigma_{1f}(+)$	$\sigma_{1f}(-)$	$\sigma_{2f}(+)$	$\sigma_{2f}(-)$	σ_{peel}	σ_{13f}	σ_{23f}
Data (MPa)	270.0	200.0	270.0	200.0	4.0	2.2	1.5

Note: +/− sign symbols tensile/compression strength; σ_{13f} and σ_{23f} are the core transverse shear strengths; σ_{peel} is the peeling strength at the interface; $E_{11} = E_{22} = 20.0$ GPa for the face sheet material; and $E_c = 0.000947$ GPa, $G_c = 0.440$ GPa for the core material.

3.2. Validation of the models

In this section, the above theoretical models are compared with numerical results obtained from the finite element analysis using ABAQUS and the high-order free vibration solution by Frostig and Baruch (1994). The comparisons of the frequencies among various models are listed in Table 1.

As shown in Table 1, Model C can predict the natural frequencies more accurately; while Models A and B also provide a close estimation of all the natural frequencies, corresponding to the symmetric and antisymmetric modes. The model by Frostig and Baruch (1994) can be simplified considering the assumption

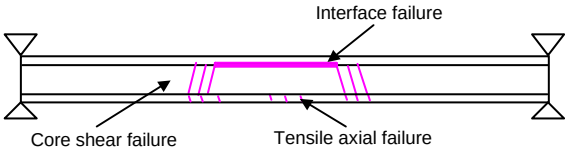

Fig. 19. The predicted failure locations and failure modes.

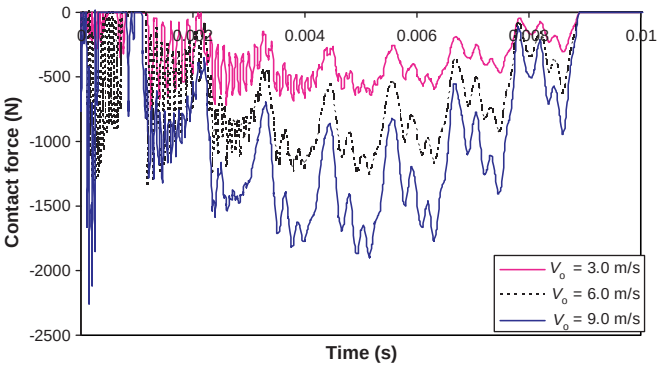

Fig. 20. Contact force history under different initial impact velocities.

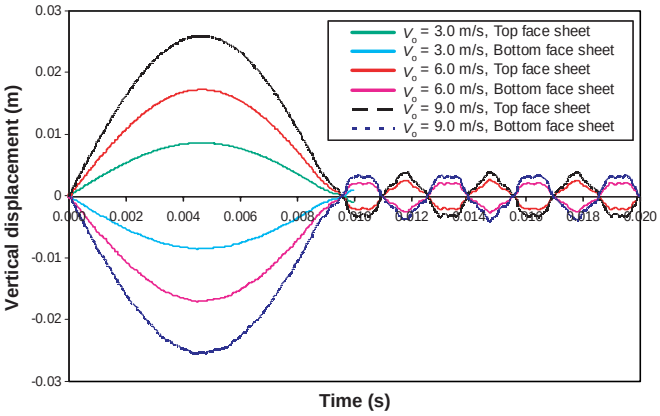

Fig. 21. Central top and bottom deflection history under different initial impact velocities.

used in their paper, in which the relation of Eq. (22) was not used. From Table 1, it indicates that the effect of rotatory inertia and horizontal vibration is very small compared to the other factors. Neglecting the

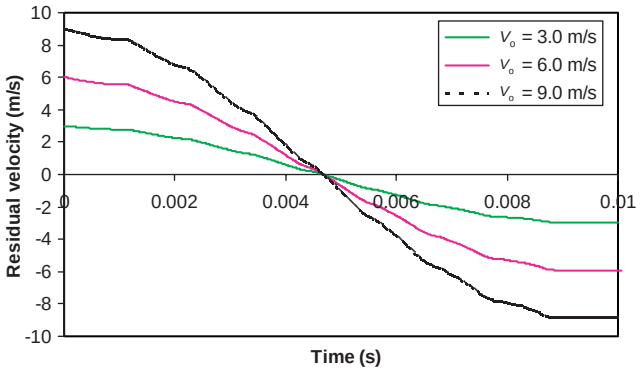

Fig. 22. Residual velocity history under different initial impact velocities.

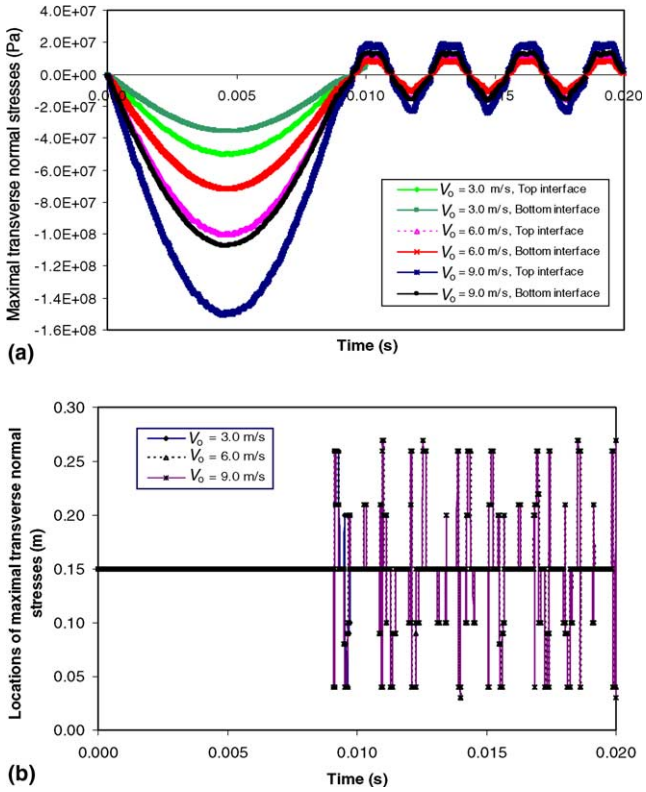

Fig. 23. Maximal transverse normal stresses at the two interfaces and the locations of the maximal transverse normal stresses under different initial impact velocities. (a) Maximal transverse normal stresses at the two interfaces. (b) Locations of the maximal transverse normal stresses happened at the top interfaces at each time step.

dynamic effect of the core material (i.e., in Model A) introduces about 10% error in the first lowest natural frequency. It is also interesting to note that inclusion of the rotatory inertia effect in Model C has a predominant influence on the third mode shape under the wave number $n = 1$ (see Table 1), which makes the uneven horizontal vibrations between the top and the bottom face sheets (Fig. 5(c)). The relatively close correlations between the natural frequencies of the three proposed models with the finite element results and the solution by Frostig and Baruch (1994) demonstrate the validity of the higher-order sandwich beam model proposed in this study, which will be next used in impact analysis.

4. Impact analysis of the symmetric sandwich beams

Based on the results shown in Table 1, Model B can be used with confidence to predict the free vibration of a symmetric sandwich beam, and it is chosen as a representative model in the impact study. A series of parametric studies are conducted considering various factors, such as impact mass, initial velocity, core height and core stiffness.

4.1. Numerical validation of the theoretical model

In order to validate the theoretical model, a LS-DYNA finite element simulation of a sandwich beam shown in Fig. 6 is set up and analyzed. The energy vs. time history in the system is shown in Fig. 7, and

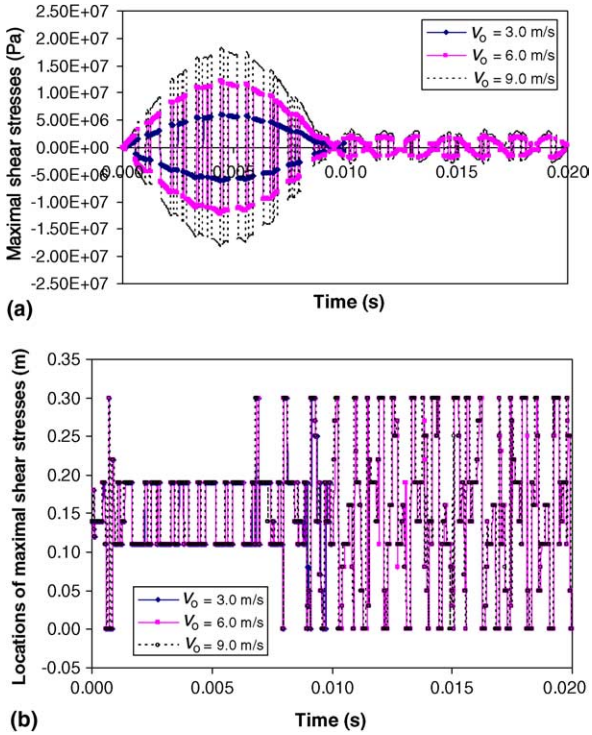

Fig. 24. Maximal shear stresses in the core and the locations of the maximal shear stresses under different initial impact velocities. (a) Maximal shear stresses in the core. (b) Locations for the maximal shear stresses happened in the core at each time step.

it indicates that the energy in the system is conservative and the sliding energy is close to zero. Therefore, the finite element model is well designed for the validation.

The contact force history, central displacement history, and residual velocity history as well as the maximal axial force history obtained with the proposed model (Model B) and the LS-DYNA simulations are compared, and the comparative results are shown in Figs. 8–11, respectively. From all the comparisons, it is noted that the proposed theoretical model captures the contact force history and the contact duration very accurately (Fig. 8), and the model also provided a close estimation over the maximal axial force history in the top face sheet (Fig. 11). Therefore, it can be concluded that the theoretical model developed in this study has comparable accuracy to the LS-DYNA simulation and can be used effectively in impact analysis and design of sandwich structures.

4.2. Impact parametric study

In this section, a parametric study of a sandwich beam subjected to impact loading is conducted, and the effects of varying the different parameters, such as impact mass, initial velocity, and core properties, on the impact process are investigated using the proposed model (i.e., Model B).

4.2.1. Effect of impact mass

The mass of the projectile or impactor is an important factor affecting the impact process and the design of a collision protective system. Applying Model B and using the same properties of the sandwich beam

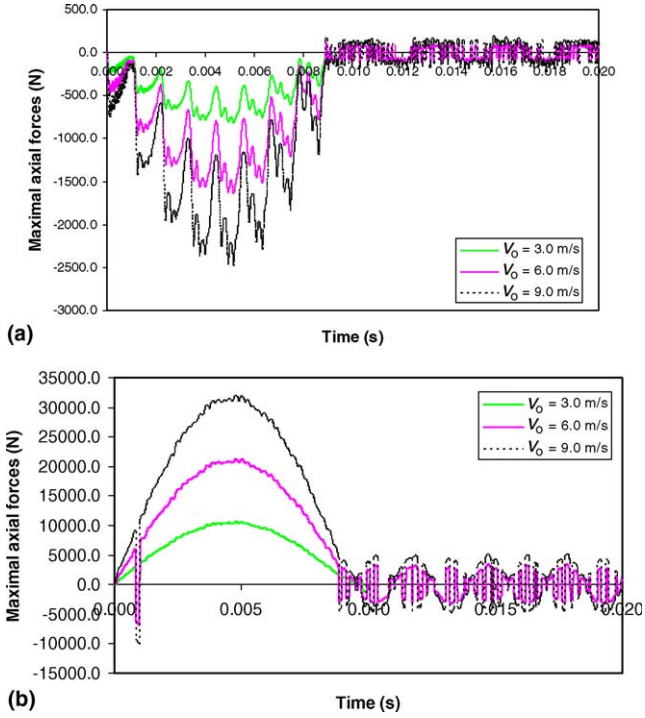

Fig. 25. Maximal axial force history in the two face sheets under different initial impact velocities. Maximal axial stresses history in the top face sheet (a) and bottom face sheet (b).

shown in Fig. 2, the effect of projectile mass is studied. Three different projectile masses of 300 g, 500 g, and 1000 g with a constant initial impact velocity of $V_0 = 3.0$ m/s are considered in the analysis.

Based on the contact force history shown in Fig. 12, the contact force reaches the maximum when the projectile mass is 1000 g, and the maximal contact force increases about 1.40 times each time when the impact mass is doubled, which is close to the linear solution previously developed by the authors (Qiao et al., 2004). Because the projectile introduces a complicated contact process with the sandwich beam, the projectile keeps adjusting its contact with the sandwich beam and makes the contact force curve unsmooth. From the deflection history of the sandwich system (Fig. 13), it is obtained that all the three projectile mass cases display as an undamped vibration state after the projectile leaves the sandwich beam completely, and the core keeps extending and contracting at the different time states with the almost same amplitude.

In Fig. 14, the residual velocity histories for the three cases of projectile masses are provided. Although the three projectile mass cases almost arrive at the same residual velocity at the end, they reach to the residual velocities in different paths. Thus, the largest mass (i.e., $m = 1000$ g) produces the longest contact duration but the slowest de-acceleration because the largest mass impacts the sandwich beam with the highest kinetic energy.

The drop weight always introduces barely visible impact damages (BVID) to the system, which makes the stress analysis generated by a drop weight especially important. The proposed higher-order sandwich impact theory offers the unique capability of analyzing the transverse normal stress (e.g., the peel stress) between the two face sheet–core interfaces, the shear stresses in the core and in the face sheets, and the axial

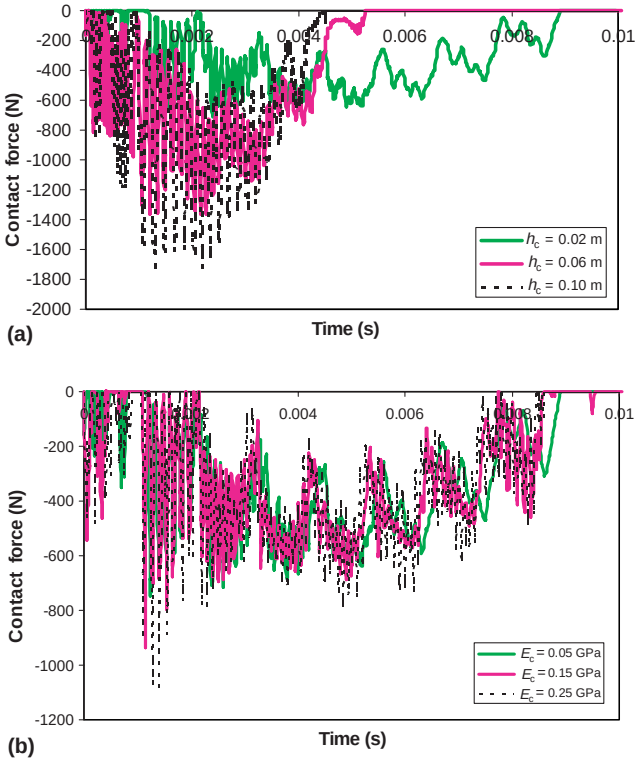

Fig. 26. Comparison of contact force history for different core heights (a) and core stiffnesses (b).

stresses generated in the face sheets, which are necessary in determining the failure modes as well as the failure locations of a sandwich system subjected to foreign object (drop weight) impact. As an illustration, the displacement and various stresses as well as the core compression generated at different times for the case of $m = 500$ g and $V_0 = 3.0$ m/s are predicted by Model B and shown in Fig. 15.

To the three projectile mass cases discussed above, the maximal transverse normal stresses, the maximal shear stresses as well as the maximal axial stress generated are plotted in Figs. 16–18, respectively, from which the locations of the maximal stresses corresponding to each time step are also shown.

Based on Fig. 16, the maximal transverse normal stress mostly occurs at the central span location of the beam before the projectile is totally separated from the sandwich beam, but it propagates to other locations as soon as the contact process is completed. As shown in Fig. 17, the maximal shear stresses mostly occurred at $x = 0.12$ and $x = 0.18$, which indicate the probable locations of core shear failure when the core shear stress reaches the core shear strength. According to Figs. 17 and 18, the wave generated by the impact can be interpreted as a combination of shear and axial stress components. Also from Figs. 17 and 18, we note that the axial wave always propagates faster than the shear wave, and the increase of impact mass increases the propagating velocity of the maximal shear stresses of the core as well as the axial stresses of the face sheets in the sandwich beam (Note: The wave speed of propagation stresses is calculated by the time of flight between two initial start peaks. From the variation of various stresses, the different propagating speeds can be observed for different stress waves.)

Given the strength data of a sandwich system like these shown in Table 2, the corresponding locations of the damages as well as the failure patterns can be derived based on the stresses calculated by the present

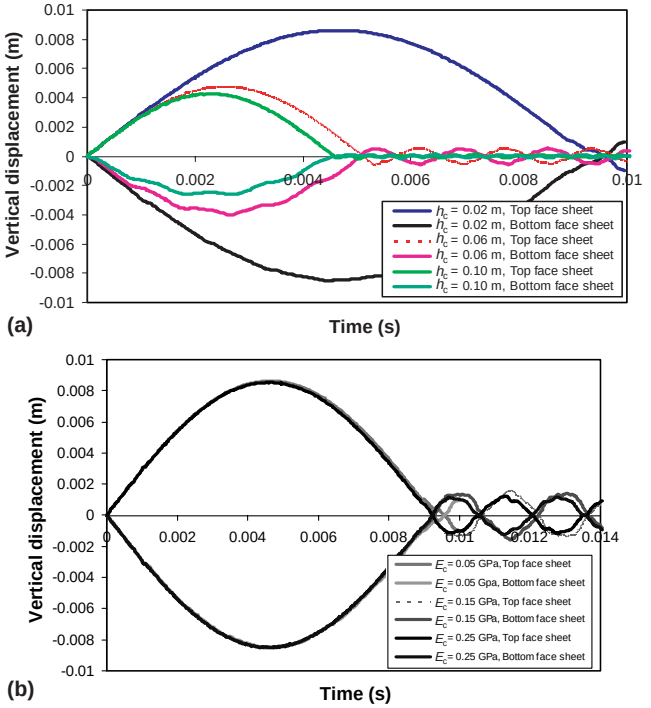

Fig. 27. Central top and bottom deflection history for different core heights and core stiffnesses. (a) Comparison of central top deflection history for different core heights. (b) Comparison of central bottom deflection history for different core stiffness.

model. Based on the predicted results from the present model, the various damages occurring at $t = 0.15 \times 10^{-3}$ is predicted when the sandwich system is subjected to an impact of a mass of 500 g. The location for debonding of the top face sheet from the core occurs at the central location (Fig. 16). At the same time, the core shear failure develops at about $x = 0.120$ m and 0.183 m (Fig. 17). The tensile failure is also observed at the bottom face sheet (Fig. 18). The failure pattern predicted by the present model is very close to those given in the literature (Abrate, 1997; Mines et al., 1998), and the predicted failure pattern is graphically illustrated in Fig. 19.

4.2.2. Effect of initial impact velocity

The initial velocity is also an important factor affecting the impact process and the design of a collision protective system. Using Model B with the same sandwich beam as studied before (Fig. 2), the effect of initial velocities is studied. Three different velocities of 3.0 m/s, 6.0 m/s and 9.0 m/s are considered in this study.

From the contact force history curves (Fig. 20), the contact force reaches its maximum when the velocity is 9.0 m/s compared to the other two velocities, and the maximal contact force increases about 2.0 times when the initial velocity increases from 3.0 m/s to 6.0 m/s and around 1.5 times when the initial velocity raises from 6.0 m/s to 9.0 m/s, which is very close to the linear solution by the authors (Qiao et al., 2004). The contact durations for these three velocities are very close to each other, which is similar to the conclusion provided by the linear solution, i.e., the contact duration time is not related to the initial

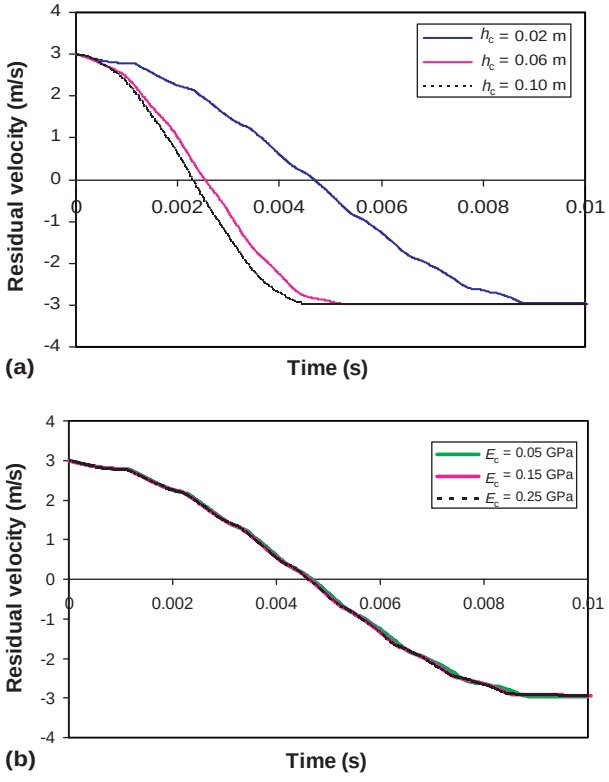

Fig. 28. Comparison of residual velocity history for different core heights (a) and core stiffnesses (b).

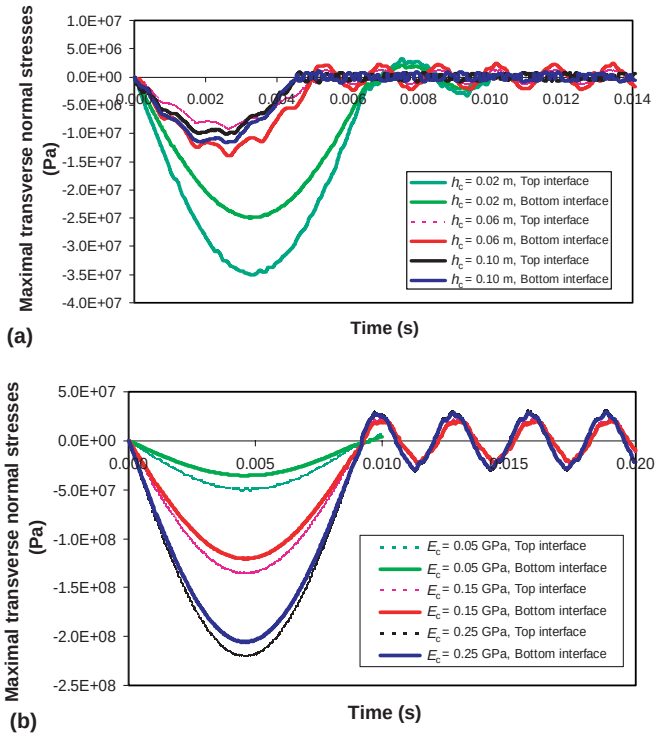

Fig. 29. Comparison of maximal transverse normal stress history for different core heights (a) and core stiffnesses (b).

velocity, but to the impact mass (Qiao et al., 2004). However, the non-linear impact process and the unsmoothed contact force history are captured by the present model (see Fig. 20).

From the deflection history of the sandwich system (Fig. 21), although the amount of the deflection is different, the pattern of the deflection shape remains similar; because no matter what theory we employ, the sandwich still behaves like a linear elastic system. It can also be observed from Fig. 21 that the higher the initial velocity, the larger the deflection.

From the residual velocity history (Fig. 22), although the pattern of the de-acceleration is similar, the highest de-acceleration is associated with the highest initial velocity, and it reaches the final residual velocities almost at the same time.

The stresses in the sandwich system under three different impact velocities are also studied. From Fig. 23(a), we note that the higher the initial velocity, the larger the transverse normal stress results. Most of time, the maximal stress happens at the center location of the beam, but it can happen at other locations as well (Fig. 23(b)). The top interface always generates a higher transverse normal stress, which makes the top skin–core interface vulnerable to debonding.

From Figs. 24 and 25, we note that the higher the initial velocity, the larger the shear and axial stresses become. Also the increase of initial velocities will increase the propagating velocities of the maximal shear and axial stresses over the beam.

4.2.3. Effect of core height (h_c) and core stiffness (E_c)

The material properties of the sandwich system itself have a significant effect on the impact process, and they are highly important in relation to the design of a collision protective system. Based on Model B and

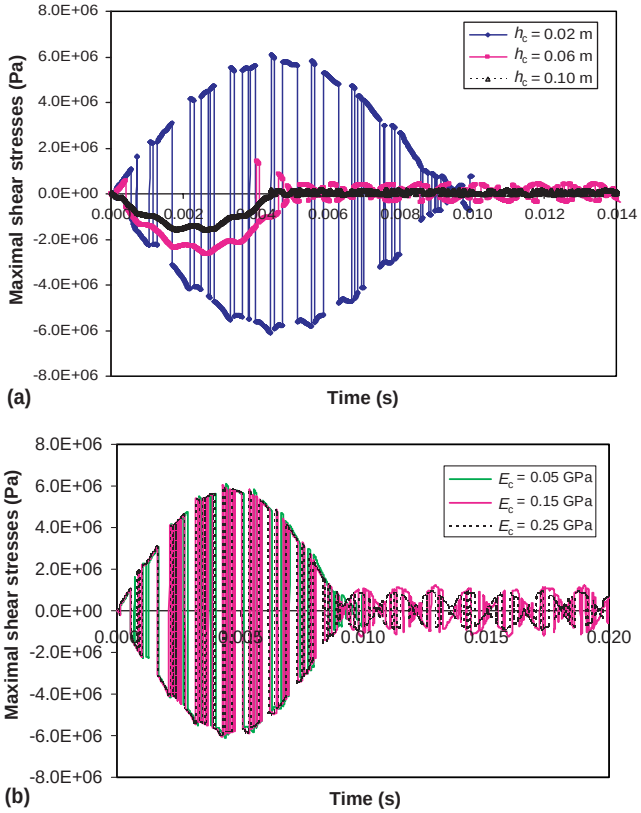

Fig. 30. Comparison of maximal shear stress history for different core heights (a) and core stiffnesses (b).

the material properties of the sandwich beam given in Fig. 2, the effects of core height and stiffness on the impact process are investigated.

From Figs. 26 and 27, we observe that the core height h_c has a prominent effect on the impact response of the sandwich system. The increase of core height results in an increased peak contact force (Fig. 26(a)) and a reduced center deflection (Fig. 27(a)) because the global bending and shear stiffnesses increase with the increase of core height. The responses of the simply-supported sandwich system (Fig. 2) given in this study are actually different from the fully-backed sandwich case discussed by the authors (Yang and Qiao, 2005). The global behavior is dominant for a simply supported sandwich, while the local behavior is more prominent for a fully-backed sandwich. Accordingly, the effect of core stiffness is also analyzed. An increase of core stiffness increases the peak contact force (Fig. 26(b)) and reduces the deflection (Fig. 27(b)). The increase of core stiffness shortens the contact duration (Fig. 26). However, this effect is less significant when the core stiffness becomes larger. The residual velocity history of the projectile is shown in Fig. 28, in which the core stiffness does not show much influence upon the residual velocities, while the core height does have a predominant effect.

Considering the transverse normal, shear and axial stresses generated, the higher the core height, the less these stress components (Figs. 29(a), 30(a), 31(a) and (b)). However, opposite to the effect of core heights, the higher the core stiffness, the higher the transverse normal stress becomes (Fig. 29(b)). It is interesting to note that the core stiffness does not show much influence on the maximal shear stress history (Fig. 30(b)) and the maximal axial stress history (Fig. 31(c) and (d)).

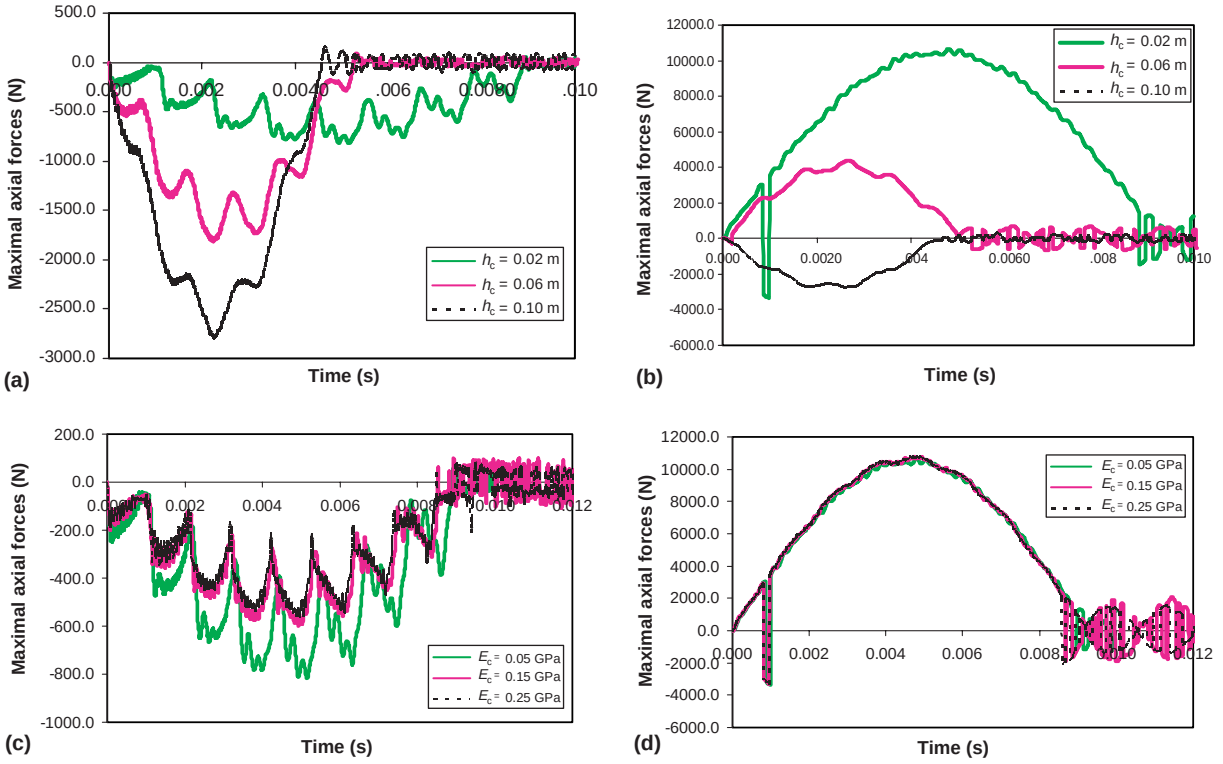

Fig. 31. Maximal axial force history for different core heights and core stiffnesses. Comparison of maximal axial force history of the top face sheet (a) and bottom face sheet (b) for different core heights. Comparison of maximal axial force history of the top face sheet (c) and bottom face sheet (d) for different core stiffnesses.

5. Conclusions

In this study, a higher-order sandwich impact theory is presented, and a detailed study has been carried out to discuss the free vibration as well as the foreign object impact problem of a sandwich beam with a soft core.

The free vibration problem considering the dynamic effect of the core, horizontal vibration and rotatory inertia is solved, and its solution is compared with the results of ABAQUS finite element simulations and the model by Frostig and Baruch (1994). It indicates that neglecting the dynamic effect of the core introduces about 10% error in predicting the first natural frequency, while including the rotatory inertia and horizontal vibration does not improve the first natural frequency much.

The foreign object impact process is further analyzed, based on the proposed higher-order sandwich beam theory. The effects of various factors, such as the projectile mass, initial impact velocity, core height and core stiffness, are discussed. The transverse normal, shear and axial stresses generated by the impact process are calculated as well and used to predict the failure patterns and locations. The parametric study of various factors on the impact process shows that the effects of mass and initial velocity over the transient impact response of the sandwich beam are close to those of the linear impact solution (Qiao et al., 2004), but the present model is capable of capturing the non-linear impact process and unsmoothed contact force history; while the core height produces a different influence on the transient impact response of the sandwich beam compared to the fully-backed case (Yang and Qiao, 2005) due to its predominant global

behavior resulting from the simply-supported boundary used in the present model. The higher-order impact sandwich theory proposed in this study improves the accuracy of sandwich analysis over impact and can be used effectively as a versatile tool to analyze, design and optimize the collision protective sandwich structures.

Acknowledgments

This study is partially supported by the National Science Foundation (EHR-0090472) and the Federal Highway Administration (FHWA) and Ohio Department of Transportation (ODOT) (State Job No. 134142). The opinions and findings, however, are those of the authors and do not necessarily reflect the views of the sponsoring agencies.

References

Abrate, S., 1997. Localized impact on sandwich structures with laminated facings. Applied Mechanics Review 50 (2), 69–82.

Allen, H.G., 1969. Analysis and Design of Structural Sandwich Panels. Pergamon, London.

Frostig, Y., Baruch, M., 1994. Free vibration of sandwich beams with a transversely flexible core: a high order approach. Journal of Sound and Vibration 176 (2), 195–208.

Frostig, Y., Baruch, M., 1996. Localized load effects in high-order bending of sandwich panels with flexible core. Journal of Engineering Mechanics 122 (11), 1069–1076.

Frostig, Y., Shenar, Y., 1995. High-order bending of sandwich beams with a transversely flexible core and unsymmetrical laminated composite skins. Composites Engineering 5 (4), 405–414.

Frostig, Y., Thomsen, O.T., 2004. High-order free vibration of sandwich panels with a flexible core. International Journal of Solids and Structures 41, 1697–1724.

Frostig, Y., Baruch, M., Vilnay, O., Sheinman, I., 1992. High-order theory for sandwich-beam behavior with transversely flexible core. Journal of Engineering Mechanics 118 (5), 1026–1043.

Lee, L.J., Kuang, K.Y., Fann, Y.J., 1993. Dynamic responses of composite sandwich plate impacted by a rigid ball. Journal of Composite Materials 27 (13), 1238–1256.

Mines, R.A.W., Worrall, C.M., Gibson, A.G., 1998. Low velocity perforation behavior of polymer composite sandwich panels. International Journal of Impact Engineering 21 (10), 855–879.

Qiao, P.Z., Yang, M.J., 2004. Static and nonlinear impact analysis of free-free sandwich plates sitting on a solid half-space. Journal of Sandwich Structures and Materials (under review).

Qiao, P.Z., Yang, M.J., Mosallam, A.S., 2004. Impact analysis of I-Lam sandwich system for over-height collision protection of highway bridges. Engineering Structures 26 (7), 1003–1012.

Sokolinsky, V.S., Nutt, S.R, 2002. Boundary condition effects in free vibrations of higher-order soft sandwich beams. AIAA Journal 40 (6), 1220–1227.

Sokolinsky, V.S., Nutt, S.R., 2004. Consistent higher-order dynamic equations for soft-core sandwich beams. AIAA Journal 42 (2), 374–382.

Thomsen, O.T., 1995. Theoretical and experimental investigation of local bending effects in sandwich plates. Composite Structures 30, 85–101.

Tsai, C.Z., Wu, E.B., Luo, B.H., 1998. Forward and inverse analysis for impact on sandwich panel. AIAA Journal 36 (11), 2130–2136.

Yang, M.J., Qiao, P.Z., 2005. Nonlinear impact analysis of fully-backed composite sandwich structures. Composites Science and Technology 65 (3–4), 551–562.